Toxicological effects of ambient fine (PM2.5-0.18) and ultrafine (PM0.18) particles in healthy and diseased 3D organo-typic mucocilary-phenotype models

J. Sotty, G. Garçon, F.-O. Denayer, L.-Y. Alleman, Y. Saleh, E. Perdrix, V. Riffault, P. Dubot, J.-M. Lo-Guidice, L. Canivet

TOXICOLOGICAL EFFECTS OF AMBIENT FINE ($PM_{2.5-0.18}$) AND ULTRAFINE ($PM_{0.18}$) PARTICLES IN HEALTHY AND DISEASED 3D ORGANO-TYPIC MUCOCILARY-PHENOTYPE MODELS

SOTTY J.[1], GARÇON G.[1], DENAYER F-O.[1], ALLEMAN L-Y.[2], SALEH Y.[1], PERDRIX. E.[2], RIFFAULT V.[2], DUBOT, P.[3], LO-GUIDICE J-M.[1], CANIVET L.[1]

[1] CHU Lille, Institut Pasteur de Lille, EA4483-IMPacts de l'Environnement Chimique sur la Santé (IMPECS), Univ. Lille, Lille, France.

[2] IMT Lille Douai, Univ. Lille, SAGE - Département Sciences de l'Atmosphère et Génie de l'Environnement, 59000 Lille, France

[3] MCMC - ICMPE UMR 7182, rue H. Dunant, 94320 Thiais, France

Corresponding author: Guillaume GARÇON, EA4483-IMPacts de l'Environnement Chimique sur la Santé Humaine (IMPECS), Institut Pasteur de Lille, CHU Lille, Univ. Lille, Lille, France, Phone number: +33-320626818, E-mail: guillaume.garcon@univ-lille.fr

ABSTRACT

The knowledge of the underlying mechanisms by which particulate matter (PM) exerts its health effects is still incomplete since it may trigger various symptoms as some persons may be more susceptible than others. Detailed studies realized in more relevant *in vitro* models are highly needed. Healthy normal human bronchial epithelial (NHBE), asthma-diseased human bronchial epithelial (DHBE), and COPD-DHBE cells, differentiated at the air-liquid interface, were acutely or repeatedly exposed to fine (i.e., $PM_{2.5-0.18}$, also called FP) and quasi-ultrafine (i.e., $PM_{0.18}$, also called UFP) particles. Immunofluorescence labelling of pan-cytokeratin, MUC5AC, and ZO-1 confirmed their specific cell-types. Baselines of the inflammatory mediators secreted by all the cells were quite similar. Slight changes of TNFα, IL-1β, IL-6, IL-8, GM-CSF, MCP-1, and/or TGFα, and of H3K9 histone acetylation supported a higher inflammatory response of asthma- and especially COPD-DHBE cells, after exposure to FP and sepcially UFP. At baseline, 35 differentially expressed genes (DEG) in asthma-DHBE, and 23 DEG in COPD-DHBE, compared to NHBE cells, were reported. They were involved in biological processes implicated in the development of asthma and COPD diseases, such as cellular process (e.g., *PLA2G4C, NLRP1, S100A5, MUC1*), biological regulation (e.g., *CCNE1*), developmental process (e.g., *WNT10B*), and cell component organization and synthesis (e.g., KRT34, COL6A1, COL6A2). In all the FP or UFP-exposed cell models, DEG were also functionally annotated to the chemical metabolic process (e.g., CYP1A1, CYP1B1, and CYP1A2) and inflammatory response (e.g., EREG). Another DEG, *FGF-1*, was only down-regulated in asthma and specially COPD-DHBE cells repeatedly exposed. While *RAB37* could help to counteract the down-regulation of *FGF-1* in asthma-DHBE, the deregulation of *FGR, WNT7B, VIPR1*, and *PPARGC1A* could dramatically contribute to make it worse in COPD-DHBE cells. Taken together, these data contributed to support the highest effects of UFP versus FP and highest sensitivity of asthma- and notably COPD-DHBE versus NHBE cells.

KEYWORDS: Fine and ultrafine particles; human bronchial epithelial cells; healthy and diseased phenotype; inflammation; transcriptomic profiling; signaling pathways

FUNDINGS

The research described in this article benefited from grants from the Hauts-de-France Region Council (Convention n°13004366). The EA4483-IMPacts de l'Environnement Chimique sur la Santé (IMPECS) of the Lille University participates in the CLIMIBIO project, which is financially supported by the Hauts-de-France Region Council, the French Ministry of Higher Education and Research, and the European Regional Development Funds. JS received a PhD fellowship funded by Lille University.

1. INTRODUCTION

Due to associated cardiorespiratory mortality and high costs to society, ambient particulate matter (PM) emission remains a global matter of concern for the 21th century. Reported health issues seem to be mostly caused by the finest particles due to their ability to diffuse deeply in the respiratory tract, where pulmonary clearance is less effective (Oberdörster et al. 1994). Indeed, PM smaller than 2.5 µm in aerodynamic equivalent diameter (AED < 2.5 µm, also called $PM_{2.5,}$), commonly known as fine particles (FP), has the greatest effect on human health (WHO, 2016). Plenty of experimental studies have already demonstrated the lung toxicity of FP, mostly through oxidative stress-induced airway inflammation, genotoxicity, epigenetic modifications or cell cycle alterations, which could be involved in the initiation and/or exacerbation of chronic lung diseases as well as lung cancers (Abbas et al. 2010, 2016, 2019; Bocchi et al. 2016; Dergham et al. 2012, 2015; Garçon et al. 2006; Gualtieri et al. 2010, 2011; Halonen et al. 2015; Leclercq et al. 2016, 2017, 2018; Longhin et al. 2013, 2016). On the contrary, to date, only very few studies have paid close attention to PM smaller than 0.1 µm in aerodynamic equivalent diameter (AED < 0.1 µm, also called $PM_{0.1,}$), also called ultrafine particles (UFP), which can represent more than 70% of the total particle number (Peters et al. 1997). Because of their high specific surface area, UFP is likely to be more reactive with target tissues and involved in large part in the reported adverse effects of FP. Their nanometric scale increases both their deposition efficiency and their retention in the airways as well as their cellular uptake and systemic distribution (Recordati et al. 2016). However, the scientific community is still far from having a detailed mechanistic explanation of the causal relation between ambient FP and/or UFP inhalation and harmful lung effects, clearly suggested by epidemiological evidence. Most of the experimental studies have focused on the toxicity of short-term acute exposure to relatively high doses of FP although recent evidences support that the underlying mechanisms induced by long-term repeated exposures to lower and therefore more realistic doses may be different (Vales et al. 2015; Zhou et al. 2016, 2017).

Airway epithelium, which is the first line of defense against inhaled pollutants, plays a key role in initiating and orchestrating inflammatory response by recognizing pathogenic patterns and secreting inflammatory mediators (Holtzman et al. 2014). Inflammatory cytokines (e.g., tumor necrosis factor-alpha, TNFα; interleukine-1 beta, IL-1β; interleukine-6, IL-6; interleukine-8, IL-8), chemokines (e.g., monocyte chemoattractant protein 1, MCP-1, and regulated upon activation normal T cell expressed, RANTES), and growth factors (e.g., granulocyte macrophage-colony stimulating factor, GM-CSF, and transforming growth factor-alpha, TGFα) have a major role in initiating, maintaining and/or aggravating airway inflammation

(Schugila, 2015). Following injury, airway epithelium can undergo partial desquamation and loss surface integrity, but can repair and regenerate its functions by secreting extracellular matrix molecules, adhesion proteins, and promoting basal cells spreading and migration at the wound site, followed by epithelial cell proliferation and differentiation (Puchelle et al. 2006). However, some of these innate mechanisms can be gradually altered among population with chronic inflammatory lung diseases such as severe asthma or chronic obstructive pulmonary disease (COPD), by dint of repeated injuries and chronical regeneration processes (Aoshiba and Nagai 2004).

Although its role in chronic inflammatory lung diseases has been clinically established, the knowledge of the underlying mechanisms by which ambient PM exerts its harmful health effects is still incomplete and detailed *in vitro* studies are therefore, highly needed. Novel tissue engineering tools, helping in recapturing the native lung environment *ex vivo*, are now available for all the major target areas of the respiratory tract. However, clinical and basic science applications have mainly focused on the bronchial epithelium, given that numerous pathologies result from disruption of this region (Pillai et al. 2014). A large part of the toxicological studies that are interested in ambient PM are routinely using immortalized cells lines, which are transformed to enable indefinite proliferation and generally cultured in submerged monolayer to screen toxicological endpoints. These immortalized cell lines provide the researcher with an almost limitless source of material. However, the pertinence of the data produced is not ensured, as some historical cell lines may not be the cell type originally reported and the response to a same chemical can be markedly different from that in primary cells (Balharry et al. 2008). Using a more relevant *in vitro* model such as primary cells is also critical to the better understanding of toxicological mechanisms related to the exposure to ambient PM (Bérubé et al. 2010). Primary cells sourced from bronchial biopsies and differentiated at the air-liquid interface (ALI) are more physiologically relevant since there are not genetically modified and can express differentiation markers such as mucins (MUC5AC), tight junctions (zonula occludens-1, ZO-1), and adhesion proteins (E-Cadherin) (Stewart et al. 2012). They also maintain the diseased phenotypes observed *in vivo* when they are isolated from patients with asthma or COPD (Burgel et al. 2011). Accordingly, Freihsat et al. (2011) demonstrated that *in vitro* differentiated normal human bronchial epithelial (NHBE) cells secreted cytokines basally after wounding, and that specific cytokine levels were increased in diseased epithelia. Recent proteomic analyses of *in vitro* NHBE and human lung apical secretions were similar in identity and quantity to those found *in vivo* (Kesimer et al., 2009). The use of ALI cultures offers a real opportunity for the direct deposition of toxicant onto the semi-dry apical cell surfaces, a situation that better mimics the deposition of PM onto the lung surface *in vivo*. Several bronchial epithelial cell

models have been cultured at the ALI, and differences in cell morphology, biochemistry or response to test materials were observed, compared to submerged cultures (Ghio et al. 2013).

In this work, we conducted *in vitro* assays, acutely and repeatedly exposing ALI-differentiated models of healthy NHBE, or asthma- or COPD-DHBE cells to relatively low doses of fine (i.e., $PM_{2.5\text{-}0.18}$, also called FP) and quasi-ultrafine (i.e., $PM_{0.18}$, also called UFP) particles. We aimed to better evaluate and compare (i) the usefulness of healthy and diseased 3D organo-typic mucocilary-phenotype models for studying the toxicity of FP and UFP, (ii) the respective sensitivities of these healthy or diseased cell models towards FP or UFP, and (iii) the respective toxicities of FP or UFP. Hence, after having checked the effective differentiation of healthy or diseased cell models at the ALI, we first studied the cytotoxicity caused by the exposure strategies we applied to ensure the choice of doses allowing to reduce exposure as much as possible while keeping a sufficient dose to study underlying mechanisms and contribute to be as close as possible to human exposure levels. Thereafter, attention was focused on the respective ability of FP and UFP to induce inflammatory, epigenetic, and transcriptomic endpoints to better decipher the molecular underlying mechanisms possibly governing their pathogenesis. Taken together, these innovative results could offer new insights into the crucial signaling pathway-related pathogenesis of lung diseases such as asthma and COPD, arguably aggravated and/or initiated by ambient PM.

2. MATERIALS AND METHODS

2.1. Chemicals

All the culture reagents for healthy or diseased 3D organo-typic mucocilary-phenotype model differentiation were provided by LONZA (Verviers, Belgium). All the chemicals were from Sigma-Aldrich (Saint-Quentin Fallavier, France). CellTiter-Glo® Luminescent Cell Viability was from Promega (Charbonnière-les-Bains, France). Vybrant Cytotoxicity Assay Kit, Hank's Balance Salt Solution (HBSS), and all the molecular biology reagents were from Thermo-Scientific (Illkirch, France). Merck-Millipore (St Quentin-en-Yvelines, France) provided mouse monoclonal anti-human pan cytokeratin (clone PU5), mouse monoclonal anti-human MUC5AC (clone CLH2), rabbit polyclonal anti-human ZO-1 (clone 5G6.1), goat polyclonal anti-mouse antibody Alexa Fluor® 488 conjugate, goat polyclonal anti-rabbit antibody Alexa Fluor® 568 conjugate, and the MILLIPLEX® MAP Human Cytokine/Chemokine Magnetic Bead Panel-Immunology Multiplex. Histone extraction kit, and HAT and HDAC Assay kits were from Active Motif (La Hulpe, Belgium). Cell Signaling Technology (Ozyme, Montigny-le-Bretonneux, France) provided rabbit monoclonal anti-human acetyl-Histone H3 (Lys9; clone C5B11), Novus Biologicals (Bio-Techne, Lille, France) provided rabbit monoclonal anti-human Histone H3 antibody (clone 1B1-B2), and R&D Systems (Bio-Techne, Lille, France) provided rabbit polyclonal anti-mouse IgG HRP conjugated Antibody (clone HAF007) and goat polyclonal anti-rabbit IgG HRP conjugated antibody (clone NB7160). AllPrep® DNA/RNA/miRNA Universal Kits were from Qiagen (Courtaboeuf, France).

2.2. PM sampling and physicochemical characterization

Both FP and UFP sampling and physicochemical characterization methods have been already detailed by Saleh et al. (2019). Briefly, particles were collected in Dunkerque, a coastal city highly industrialized, located in the north of France. A high-volume impactor sampler has been set up to collect fine fraction (i.e., $PM_{2.5\text{-}0.18}$, with AED between 2.5 µm and 0.18 µm) by impaction, and quasi-ultrafine fraction (i.e., $PM_{0.18}$, with AED < 0.18 µm) by filtration on A4 sized-polycarbonate filter. Weekly samples were collected between September 9th, 2013 and April 14th, for 26 weeks in total, quickly stored at -20°C, and combined together. Size distribution and zeta potential were carried out by dynamic light scattering using zetasizer nano ZS (Malvern Instruments©, Malvern). After microwave mineralization under acid conditions, trace metal and metalloid concentrations of FP and PUF were carried out by inductively coupled plasma mass spectrometry (NeXion 300x, Perkin Elmer, Waltham, MA,

USA), as published by Alleman et al. (2010) and Mbengue et al. (2014). Before the analysis of surface contents by X-Ray photoelectron spectroscopy (XPS_K ALPHA, Thermo Scientific), FP and UFP were setting up on silicon wafer, introduced in primary vacuum chamber (10^{-7} mbar, 60 min) to degas, and transferred in analysis chamber (10^{-9} mbar, 320 min). Pressurized liquid extraction using a Dionex ASE 200 instrument (ThermoFisher Scientific) and extract evaporation for enrichment under a gentle stream of nitrogen in a TurboVap II water bath held at 60°C (Zymark, Roissy, France) were needed before analyzing PAH concentrations of FP and UFP by high-pressure liquid chromatography (i.e., Waters 2695 Alliance system, on-line 996-photodiode array, and a 2475-fluorimetric detector; Waters SA, Saint-Quentin-en-Yvelines, France), as published elsewhere (Crenn et al. 2017).

2.3. NHBE, and asthma- and COPD-DHBE cells and culture conditions

NHBE, and asthma- and COPD-DHBE cells were commercially available primary cells, established from biopsies isolated from four healthy, four asthma-, and four COPD-diseased donors, respectively. Table S1 shows the characteristics of all the donors and the cells (see also supplemental data). Culture conditions have been published elsewhere (Leclercq et al. 2016). Briefly, cells were grown in CellBIND® surface plastic flasks with bronchial epithelial growth medium (BEGM™; Bronchial Epithelial BulletKit™, LONZA) supplemented with 1% (v/v) penicillin/streptomycin. Once the cells have reached 80% of confluence, they were seeded at 200,000 cells/cm^2 on Transwell® polyester permeable membrane cell culture inserts (i.e., 24 mm insert diameter, tissue culture treated-polyester membrane; 0.4 µm pore diameter, 4 x 10^6 pores/cm^2; 4.67 cm^2 insert membrane growth area; 10 µm nominal membrane thickness; 0.03% (v/v) type-I collagen from rat tail membrane-coating) in 6-well Transwell® microplate supports (Costar, Corning, USA). Once cells had reached confluence, ALI conditions were established by adding 0.2% (v/v) inducer in the B-ALI™ differentiation medium (B-ALI BulletKit™, LONZA).

2.4. Immunohistochemistry

NHBE, and asthma- and COPD-DHBE cells were fixed with 1% (v/v) paraformaldehyde for 3 min at 37 °C and then methanol at -20 °C for 5 min. Thereafter, they were permeabilized for 3 min with 0.2% (v/v) Triton X-100 in phosphate-buffered solution (PBS), rinsed three times for 5 min in PBS, and incubated for 1 h at 37 °C with primary antibodies diluted in PBS containing 3% (v/v) bovine serum albumin (BSA), 0.05% (v/v) Tween, and 0.08% (v/v) sodium azide. Mouse monoclonal anti-human pan cytokeratin, mouse monoclonal anti-human

MUC5AC, and rabbit polyclonal anti-human ZO-1 were respectively diluted at 1/100, 1/250, and 1/500 (Merck Millipore). Cells were rinsed three times for 5 min in PBS and incubated for 30 min at 37 °C with a goat polyclonal anti-mouse antibody-Alexa Fluor®488 conjugate or goat polyclonal anti-rabbit antibody-Alexa Fluor® 568 conjugate, diluted at 1/400 in PBS containing 3% (v/v) BSA, 0.05% (v/v) Tween, and 0.08% (v/v) sodium azide (Merck Millipore). Cells were mounted with SlowFade® Gold Antifade Mountant with DAPI (Life Technologies) and images were acquired on a confocal scanning microscope LSM 710 (Zeiss, Oberkochen, Germany).

2.5. Transmission electron microscopy (TEM) observations

NHBE, and asthma- and COPD-DHBE cells were fixed for 20 min with paraformaldehyde-glutaraldehyde (2% v/v) in PBS, and then for 40 min by renewing the fixation solution. After a post-fixation with osmium tetroxide (1% v/v) in PBS, cells were progressively dehydrated in graded alcohols and embedded in an Epon/ethanol mixture and thereafter in Epon. Sections (85 nm) were cut and stained with uranyl acetate (2% v/v) and Reynolds lead citrate prior to their observation in TEM (Zeiss EM900, Carl Zeiss SAS, Marly le Roi, France).

2.6. Exposure strategy to FP and UFP

FP and UFP samples were suspended at 46.7 µg/mL in HBSS (Thermofisher) supplemented with 1% (v/v) amphotericin-B (250 µg/mL). Each cell lot was assigned into 5 groups: control group (i.e., exposed to vehicle solution: HBSS with 1% (v/v) amphotericin-B (250 µg/mL), FP acute exposure group (i.e., exposed to FP once for 6 h), FP repeated exposure group (i.e., exposed to FP three times for 6 h with 18 h intervals), and similarly, UFP acute exposure group (i.e., exposed to UFP once for 6 h) and UFP repeated exposure group (i.e., exposed to UFP three times for 6 h with 18 h intervals). The rationale for selection of the FP and UFP dose of 5 µg/cm² in the exposure strategy applied in this work was based on the literature reporting the harmful occurrence of oxidative stress, pro-inflammatory responses, genetic and epigenetic modifications, and/or mitochondrial function alteration in NHBE and/or COPD-DHBE cells repeatedly exposed to ambient FP and/or at relatively low doses ranging from 1 to 10 µg/cm² (Boublil et al. 2013, Leclercq et al. 2016, 2017, 2018). Just before cell exposure, FP and UFP were suspended at the expected concentrations with sterile HBSS with 1% (v/v) amphotericin-B (250 µg/mL), and twice sonicated for 2 min. After the last exposure, cell-free culture media were collected and quickly-frozen at -80°C for the future study of extracellular glucose-6-phosphate

dehydrogenase (G6PD) activity and inflammatory mediator secretion, whereas adherent cells were washed once with 1 mL-aliquots of cold sterile PBS, and either quickly prepared for microscopic observation or immunofluorescence labelling, used for the determination of intracellular ATP concentrations, quickly frozen at -80°C until the future determination of the histone acetyltransferase (HAT) and deacetylase (HDAC) activities and histone post-translational modifications, or quickly lysed in QIAzol lysis reagent (Qiagen) and frozen at -80°C until the future determination of transcription expression profiles.

2.7. Toxicological endpoints

2.7.1. Cytotoxicity: Viability of FP and UFP-exposed NHBE, and asthma- and COPD-DHBE cells was evaluated through the determination of intracellular ATP concentration (CellTiter-Glo® Luminescent Cell Viability, Promega) and G6PD activity (Vybrant Cytotoxicity Assay Kit, ThermoFisher Scientific).

2.7.2. Inflammatory mediators: Concentrations of TNFα, IL-1β IL-6, IL-8, GM-CSF, MCP-1, RANTES, and TGFα have been investigated in cell-free culture media using MILLIPLEX® MAP Human Cytokine/Chemokine Magnetic Bead Panel-Immunology Multiplex Assay, according to the manufacturer's recommendations (Merck-Millipore; Blasco et al. 2017).

2.7.3. Histone post-translational modification: HAT and HDAC activities were analyzed using HAT Assay kit and HDAC Assay kit (Active Motif). Histone extracts (3 µg), prepared using commercially available histone extraction kit (Active Motif), were separated by electrophoresis on SDS-PAGE gels and then transferred on nitrocellulose membranes. After their blockage in 5% non-fat dry milk for 45 min, membranes were incubated firstly with primary antibodies (i.e., rabbit monoclonal anti-human acetyl-Histone H3 (Lys9), Cell Signaling Technology, and rabbit monoclonal anti-human Histone H3 antibody, Novus Biological) overnight at 4°C, secondly for 1 h with secondary antibodies (i.e., rabbit polyclonal anti-mouse IgG HRP conjugated antibody and goat polyclonal anti-rabbit IgG HRP conjugated antibody, R&D systems) at room temperature, and at least with ECL prime Western Blotting Detection reagent (GE Healthcare). Chemiluminescence was detected by Fusion FX Spectra (Vilbert-Lourmat, Marne-la-Vallée, France).

2.7.4. Gene expression: Gene expression analysis was carried out by using microarrays. Briefly, total RNA contents were extracted using the AllPrep® DNA/RNA/miRNA Universal Kit (Qiagen®, Courtaboeuf, France), and total RNA yield and quality were further assessed on the Agilent 2100 bioanalyzer (Agilent Technologies, Massy, France). After the reverse transcription, one color whole Human (039494 slides) 60-mer oligonucleotides 8x60k microarrays (Agilent Technologies) were used to analyze gene expression. cRNA

labelling, hybridization and detection were carried out according to supplier's instructions (Agilent Technologies). For each microarray, Cyanine 3-labeled cRNA were synthesized with the low input QuickAmp labeling kit from 25 ng of total RNA. RNA Spike-In were added to all tubes and used as positive controls of labelling and amplification steps. The labelled cRNA were purified and 600 ng of each cRNA were then hybridized and washed following manufacturer's instructions. Microarrays were scanned on an Agilent G2505C scanner and data extracted using Agilent Feature Extraction Software© (FE version 10.7.3.1). Raw intensities from all sample were converted to log2, normalized to the 75th percentile, and probes under background were eliminated. Statistical analyses were performed with linear models for microarray data package version 3.22.7 (Ritchie et al. 2015) using the moderated t statistics with normalized data. Given the low exposure dose and small sample sizes used in this study, and since our objective was to identify more differentially expressed genes (DEG) in each group, selected DEG were those with a raw p value < 0.01 and absolute fold change (FC) > 1.5.

2.7.5. Signaling pathways: Gene function analysis was done by using the PANTHER classification system, version 13.1 (Mi et al. 2013) based on the gene ontology (GO) consortium database. Enrichment analysis was performed with the freely available web-based tool Enrichr (http://amp.pharm.mssm.edu/Enrichr) (Kuleshov et al. 2016) to identify statistically deregulated pathways on the basis of Kyoto Encyclopedia of Genes and Genomes (KEGG) database (Fisher exact test, adj *p* value < 0.05). The gene interaction networks were generated through the use of Ingenuity Pathway Analysis (Qiagen, Courtaboeuf, France).

2.8. Statistical analyses

Statistical comparisons were achieved with GraphPad Prism version 7.0. A non-parametric test of Kruskal Wallis with a post hoc test of Dunn's for multiple comparison correction have been used to compare the different conditions (i.e., exposed versus control cells, asthma- or COPD-DHBE group versus NHBE group). Results were considered significant when adjusted *p* value < 0.05.

3. RESULTS

3.1. Physicochemical characteristics of FP and UFP

Both FP and UFP physicochemical characterization have been already detailed by Saleh et al. (2019). The UFP represented 10.5% of the total FP fraction mass estimated over the sampling period. This percentage was higher than the usual values (i.e., < 5%) encountered in ambient air probably because of the inclusion of particles slightly larger than the typical UFP and the localization of the high-volume impactor sampler near at once large industries and heavily trafficked roads. The size distribution showed a monomodal distribution for FP (i.e., 1265 ± 239 nm), and a bimodal distribution for UFP, (i.e., 188.0 ± 39.9 nm and 1078 ±305 nm), corresponding to UFP and UFP aggregates, respectively. Particle surface analysis revealed quite similar atomic compositions of FP and UFP with the presence, according to decreasing proportions, of C, O, Cl, Si, N, S, and Ca (Figure S1, see also supplemental data). As shown in Table 1, FP and UFP have quite similar elemental compositions; however, some variations in the enrichment degree of certain elements (i.e., Mn and Zn for FP, and As, Ni, Pb, and V for UFP) were reported. Because of the use of HBSS, the concentrations of Na, Mg, and K in UFP could not be considered. Total element concentrations, without Na, Mg, and K, in FP and UFP were 50,572 µg/g and 36,097 µg/g, respectively. As shown in Table 2, PAH profiles were almost similar in both FP and UFP; nonetheless, a slight increase (10%) of total PAH concentrations was reported in FP. In FP and UFP, total PAH concentrations were 94 µg/g and 84 µg/g, respectively, whereas BaP concentrations were 3.8 µg/g and 5.3 µg/g, respectively.

3.2. NHBE and COPD-DHBE cells differentiation

The effective differentiation into bronchial epithelia of NHBE, and asthma- and COPD-DHBE cells at the ALI was checked (Figure 1). Cells were firstly cultivated in immerged conditions until confluency (Figure 1A). After 28 days of differentiation at the ALI, cell layers formed a characteristic relief structure (Figure 1B). Ultrafine sections of differentiated cells showed ciliated areas at the apical pole of the cell layer (Figure 1C). Immunofluorescence labelling of an epithelial characteristic group of proteins, which comprised pan-cytokeratin, MUC5AC, and ZO-1, was carried out (Figure 1D, 1E, and 1F, respectively). Cytokeratin protein expression supported the epithelial cell-types of NHBE, and asthma- and COPD-DHBE cells (Figure 1D). Secretion of MUC5AC, a mucin representing one of the major lung mucus components, revealed the presence of some mucus-producing cells (Figure 1E). ZO-1 protein expression confirmed the integrity of the tight junctions, which constitute the barrier between the apical and the basolateral domains of the plasma membrane (Figure 1F).

3.3. Cytotoxicity of FP and UFP in NHBE, and asthma- and COPD-DHBE cells

The Figures 2A and 2B respectively show the intracellular ATP concentrations of NHBE, and asthma- and COPD-DHBE cells after acute or repeated exposures to FP or UFP at 5 µg/cm^2. In acutely exposed-cells, FP did not alter any ATP concentration whereas UFP slightly reduced them, with a significant change only in COPD-DHBE cells ($p < 0.05$). In repeatedly exposed-cells, both FP and UFP significantly decreased ATP concentrations in NHBE and asthma-DHBE cells, but only UFP significantly altered them in COPD-DHBE cells ($p < 0.05$). The Figures 2C and 2D respectively show the lack of any change of G6PD activity in cell-free culture media of NHBE, or asthma- or COPD-DHBE cells acutely or repeatedly exposed to FP or UFP at 5 µg/cm^2. Taken together, these results supported the use of the low-cytotoxic dose of 5 µg/cm² to apply for the further study of the toxicological endpoints in all the cell models under study.

3.4. Inflammatory mediator secretion in NHBE, and asthma- and COPD-DHBE cells

No significant difference between the levels of the inflammatory mediators secreted in cell-free culture media by the different cell models were reported at their basal states (Figure 3). Both FP and PUF exposures did not induce any significant change of their secretion by NHBE cells (Figures 4 and 5). In contrast, in cell models with diseased phenotypes, especially in COPD-DHBE ones, exposures to FP and notably UFP induced slight and sometimes statistically significant increases of the secretion of inflammatory mediators (i.e., TNFα, IL-1β, IL-6, IL-8, GM-CSF, MCP-1, and/or TGFα) as compared to their respective controls and, moreover, NHBE cells. For exemple, as shown in Figure 4-A and B, slight increases of TNFα secretion were observed in asthma-DHBE cells acutely exposed to PUF, whereas higher, even statistically significant, increases of this cytokine were seen in COPD-DHBE cells acutely or especially repeatedly exposed. Both GM-CSF and MCP-1 have almost similar secretion profiles as the one of TNFα (Figures 5-A and B, 6-A and B, respectively). As shown in Figure 4-C and -D, there were slight increases of IL-1β secretion in asthma- and COPD-DHBE cells acutely and/or repeatedly exposed to PUF and/or especially PUF. Secretion profiles of IL-6, IL-8, and TGFα were almost similar as the one of IL-1β (Figures 4-E and F, 4-G and H, and 5-G and H, respectively). Taken together, these results indicated a higher inflammatory response triggered by relatively low doses of FP and in particular UFP, but without any clear influence of the exposure strategy, in sensitive asthma- and notably COPD-DHBE cells. However, the above-reported trends were generally non significant due to the relatively high intra-variability of the inflammatory mediator secretion within each cell model.

3.5. HAT and HDAC activities, and H3K9 histone acetylation in NHBE, and asthma- and COPD-DHBE cells

The Figure 6 shows both HAT and HDAC activities in NHBE, and asthma- and COPD-DHBE cells, acutely and repeatedly exposed to either FP or UFP. In all the cell models, but especially COPD-DHBE cells, exposure to both FP and in particular UFP induced a slight trend to HDAC activity reduction, resulting in a slight trend to HAT/HDAC ratio increase. A slight trend to H3K9 histone acetylation was seen in asthma- and especially COPD-DHBE cells, acutely and/or rather repeatedly exposed to FP and/or in particular UFP. For exemple, HDAC activity was slightly decreased and H3K9 histone acetylation slightly increased in COPD-DHBE cells repeatedly exposed to PUF (Figures 6-D and H, respectively). Overall, these results indicated a slight trend of HDCA activity reduction thereby resulting in H3K9 histone acetylation triggered by FP and in particular UFP, but without any clear influence of the exposure strategy, in all the cell models but rather in sensitive COPD-DHBE cells. However, one more time, the above-reported changes were generally non significant due to the relatively high intra-variability within each cell models.

3.6. Gene expression profiles in NHBE, and asthma- and COPD-DHBE cells

To better characterize diseased cell phenotypes, DEG between asthma- or COPD-DHBE, and NHBE cells, at baseline were first analyzed (i.e., see also supplemental data for complete gene lists, Table S2). Indeed, 35 DEG (i.e., 16 up- and 19 down-regulated) were reported in control asthma-DHBE, and 23 DEG (i.e., 11 up- and 12 down-regulated) in control COPD-DHBE, compared to control NHBE cells.

Thereafter, pan-transcriptomic data of NHBE, or asthma- or COPD-DHBE cells acutely or repeatedly exposed to FP and PUF were compared to their respective controls. The almost similarity between the gene expression patterns reported in all the cell models after both FP and UFP exposures supported the choice to limit future analyses only on the DEG triggered by UFP (i.e., see also supplemental data for complete gene lists, Table S3). In NHBE cells, 32 (i.e., 23 up- and 9 down-regulated) and 57 (i.e., 39 up- and 18 down-regulated) DEG were reported, respectively after acute and repeated exposures (Table 3). There were respectively 56 (i.e., 45 up- and 11 down-regulated) and 43 (i.e., 27 up- and 16 down-regulated) DEG in asthma-, and 73 (i.e., 62 up- and 11 down-regulated) and 67 (i.e., 52 up- and 15 down-regulated) in COPD-DHBE cells (Tables 4 and 5). The number of DEG was quite higher in asthma and rather COPD-DHBE cells than those in NHBE cells (Figure 7).

As shown in Figure 7, respectively 9 (i.e., *cytochrome P4501A1: CYP1A1, neuronal pentraxin 1: NPTX1, cytochrome P4501B1: CYP1B1, Solute Carrier Family 7 Member 5: SLC7A5, Ectonucleoside Triphosphate*

Diphosphohydrolase 8: ENTPD8, G Protein-Coupled Estrogen Receptor 1: GPER1, Receptor tyrosine kinase-like orphan receptor 1: ROR1, Enhancer of mRNA-decapping protein 3: EDC3, and *Transmembrane Protein 138: TMEM138*) and 10 (i.e., *CYP1A1, cytochrome P4501A2: CYP1A2, CYP1B1, Cysteine Rich Tail 1: CYSRT1, Long Intergenic Non-Protein Coding RNA 886: LINC00886, Transmembrane Protein 156: TMEM156, MFNG O-Fucosylpeptide 3-Beta-N-Acetylglucosaminyltransferase: MFNG, Epiregulin: EREG,* and *Enhancer Of MRNA Decapping 3: EDC3, KIT Ligand: KITLG*) DEG were reported as common to all the cell models acutely or repeatedly exposed to UFP. In addition, respectively 6 (i.e., EREG, *LINC00886, Solute Carrier Family 45 Member 4: SLC45A4, TCDD Inducible Poly(ADP-Ribose) Polymerase: TIPARP, Slingshot Protein Phosphatase 1: SSH1, FOS Like 1,* and *AP-1 Transcription Factor Subunit: FOSL1*) and 8 (i.e., *ENTPD8, Acyl-CoA Oxidase Like: ACOXL, TIPARP, LOC284072, SLC45A4, FOSL1, Cbp/P300 Interacting Transactivator With Glu/Asp Rich Carboxy-Terminal Domain 2: CITED2,* and *Fibroblast Growth factor 1: FGF1*) DEG were reported as common to both the DHBE cell models acutely or repeatedly exposed.

Gene ontology (GO) analyzes were used to identify main molecular functions of DEG and the biological processes in which they are involved. As shown in Figures 8-A and 8-B, the biological processes (e.g., biological process cellular process, metabolic process, biological regulation, response to stimulus, developmental process) and molecular functions (e.g., binding, catalytic activity, transporter activity, receptor activity, signal transducer activity) activated by the repeated exposures to PUF were quite similar to those triggered by acute exposure to PUF in all the cell models. Interestingly, the numbers of DEG involved in them were higher in COPD- than in asthma-DHBE and NHBE cells. Some biological processes (e.g., immune system process, biological adhesion, locomotion) and molecular functions (e.g., translation regulatory activity) were activated only in diseased and particularly COPD-DHBE cells.

The network classification system of IPA software was used to identify gene clusters in term of interactions between them and causal relationships. Despite some slight differences between the cell models (i.e., NHBE and asthma-DHBE vs COPD-DHBE) and exposure strategies (i.e., acute vs repeated), top networks were generally associated with inflammation (*Interleukin-24: IL-24*), AHR signaling pathway (i.e., *Aldehyde Dehydrogenase 3 Family Member A1: ALDH3A1, CYP1A1, CYP1B1, CYP1A2, NAD(P)H Quinone Dehydrogenase 1: NQO1,* and *TIPARP*), and cell cycle, cellular movement, and cell growth and proliferation (i.e., *Choline Dehydrogenase: CHDH, Epithelial Mitogen: EPGN, EREG, GPER1, FGF1, FGR Proto-Oncogene, Src Family Tyrosine Kinase: FGR, GPR110, KITLG, ROR1, SLC7A5, Stanniocalcin 2: STC2, Vasoactive Intestinal Peptide Receptor 1: VIPR1,* and *Wnt Family Member 7B: WNT7B*) (i.e., see also

supplemental data for complete top networks, Table S4). However, some specific DEG allowed to discriminate specific signaling pathways in asthma- (i.e., *FGF1* and *RAB37*) and specially COPD-DHBE (i.e., *FGF1, PPARG Coactivator 1 Alpha: PPARGC1A, FGR, WNTB7,* and *VIPR1*) cells acutely or repeatedly exposed to PUF, thereby supporting their highest sensitivity.

DISCUSSION

To be closer to realistic exposure conditions, in this work, NHBE as well as asthma- and COPD-DHBE cell models have been developed. Besides cancer-derived or immortalized cell lines, more relevant epithelial-based *in vitro* models, such as 3D organo-typic mucocilary-phenotype models, need urgently to be used because of their physiological relevance to *in vivo* (Bérubé et al. 2009; Prytherch and BéruBé, 2014). The cell culture conditions we used ensured that the three 28 days-differentiated cell models exhibit specific phenotypes with many similarity points with the *in vivo* human bronchial epithelium (Bérubé et al. 2010). Indeed, cell layers formed a characteristic relief structure and microscopy revealed the characteristic presence of mixed specific cell types such as goblet, basal, or ciliated epithelial cells (Leclercq et al. 2016, 2018). Immunofluorescence labelling of pan-cytokeratin, MUC5AC, and ZO-1 respectively supported (i) their epithelial cell-types, (ii) the ability of some of them to specifically secrete mucus, with asthma- and COPD-DHBE epithelia containing the highest number of goblet cells, and (iii) the integrity of their tight junctions (Boublil et al. 2013). However, it is noteworthy that, despite these 3D organo-typic mucocilary-phenotype models could be extremely relevant to further toxicity studies, to date, only few studies have used them to evaluate ambient FP and/or UFP toxicity.

Based on previous works, healthy and diseased cell models were acutely or repeatedly exposed to ambient FP or UFP at 5 µg/cm². The dose we applied was among the lowest reported to give harmful effects whilst limiting a massive cell death (Boublil et al. 2013; Leclercq et al. 2016, 2017, 2018). It is also of great importance to reduce PM exposure as much as possible to keep a sufficient dose allowing studying underlying mechanisms while contributing to the effort to be closer to human exposure levels.

Asthma and COPD are both characterized by chronic inflammation in the lung, but the nature and sites of the inflammation differ between diseases and also within each disease. Over 100 inflammatory mediators have been implicated in asthma and COPD, and they may have a variety of effects on the airways that in combination account for the pathological features of these diseases (Barnes et al. 2009, 2017). In this work, somewhat surprisingly, baseline secretions of inflammatory mediators by healthy and diseased cells were almost quite similar. Accordingly, Hackett et al. (2011) reported that asthmatic-derived ALI cultures responded without any significant change in the secretion of inflammatory mediators (i.e., IL-6, IL-8, and GM-CSF), compared to non-asthmatic derived ALI cultures. Leclercq et al. (2016) rather found higher constitutive levels of some of them (i.e., TNFα, IL-1β, IL-8, and GM-CSF) in COPD-DHBE in comparison with NHBE cells, thereby indicating that this diseased phenotype still conserved its basal inflammatory status. These mediators are found as increased

in COPD, because of their participation to inflammation aggravation and/or maintenance, by promoting inflammatory cell differentiation and survival, favoring structural cell proliferation and/or activation, or even recruiting inflammatory cell from the circulation (Barnes et al. 2017). The apparent discrepancy between our results and those published by Leclercq et al. (2016) might notably rely on the inter-individual variability of the cell donors, notably due to possible difference in disease stages and/or drug therapy, only limited data having been provided by the cell supplier. Both FP and UFP exposures did not induce any change of the inflammatory mediator secretion by NHBE cells. In asthma- and especially COPD-DHBE cells, both FP and UFP exposures triggered rather slight and sometimes even significant increases of almost all the inflammatory mediators (i.e., TNFα, TNFβ, IL-6, IL-8, GM-CSF, and/or TGFα). Overall, these results indicated a higher inflammatory response in diseased cells, especially COPD-DHBE cells, exposed to relatively low doses of UFP rather FP. Although the above-reported trends were generally non-significant due to the above-mentionned inter-individual variability of the cell donors, these data seemed consistent with those reported by Leclercq et al. (2016, 2018) revealing the secretion of some members of the inflammatory network mainly in COPD-DHBE cells repeatedly exposed to ambient FP. According to Lodovici and Bigagli (2011), the correlation between some redox-active compounds of PM (e.g., metals, PAH) and inflammatory events might rely on the regulation of redox sensitive transcription factors, such as nuclear factor-kappa B (NF-κB). The activation of the NF-κB pathway and the subsequent inflammatory mediator secretion have been well-demonstrated in these target cells after metal or PAH rich PM-exposure (Leclercq et al. 2018; Schuliga et al. 2015; Vales et al. 2015; Zhou et al. 2016, 2017).

In addition, despite the relatively high inter-individual variability of the cell donors, exposure to FP and rather UFP induced a slight trend to reduce HDAC activity, resulting in slight trends in H3K9 histone acetylation within diseased cells, with a greater effect within COPD-DHBE. Accordingly, HDAC activity has been reported as decreased in bronchial-biopsy from patients suffering from COPD, this latest been correlated with both the disease severity and inflammation intensity (To et al. 2016). Acetylation of lysine residues on H3 histone has been related to the gene transcription that promotes inflammation (Chen et al. 2015). Although only very few data are available about the post-translational modifications of histones induced by air pollutants, and, in particular, ambient PM, Leclercq et al. (2016, 2017) reported dose- and exposure-dependent changes of site-specific acetylation of H3 histone and HDAC activity, particularly within COPD-DHBE cells, after ambient FP exposure. Other authors closely supported that metal and/or PAH rich ambient FP contributed to dysregulated H3K9 histone acetylation (Cantone et al. 2014; Ding et al. 2017; Wang et al. 2012). Overall, despite the relatively high inter-individual variability of the cell donors, our results supported that the slight trend of H3K9

histone acetylation, mainly reported in sensitive COPD-DHBE cells repeatedly exposed to FP and UFP, could be related to the trend of the aggravation and/or maintenance of inflammation within these sensitive diseased cells.

Thereafter, to better identify the underlying pathways deregulated by ambient FP or UFP exposure in healthy or diseased cell phenotypes, a transcriptomic profiling by microarray technology has been applied. Firstly, at baseline 35 DEG (i.e., 16 up- and 19 down-regulated) in asthma-DHBE and 23 DEG (i.e., 11 up- and 12 down-regulated) in COPD-DHBE were reported, compared to NHBE cells. Interestingly, Barnes et al. (2017) reported that some of these DEG were involved in critical biological processes implicated in the development of both asthma and COPD diseases, such as cellular process (e.g., *PLA2G4C, NLRP1, S100A5, MUC1*), biological regulation (e.g., *CCNE1*), developmental process (e.g., *WNT10B*), and cell component organization and synthesis (e.g., KRT34, COL6A1, COL6A2). Despite the relatively low number of DEG, probably reflecting the relatively high inter-individual variability of the cell donors, taken together, these results indicated specific transcriptomic patterns allowing discriminating between the basal healthy and diseased cell phenotypes.

Secondly, DEG in all the FP or UFP-exposed cell models revealed almost quite similar patterns for both the size fractions. Having therefore chosen to focus attention on UFP-induced DEG patterns, respectively 9 (i.e., *CYP1A1, NPTX1, CYP1B1, SLC7A5, ENTPD8, GPER1, ROR1, EDC3, TMEM138*) and 10 (i.e., *CYP1A1, CYP1A2, CYP1B1, CYSRT1, LINC00886, TMEM156, MFNG, EREG, EDC3, KITLG*) DEG were reported as common to all the exposed-cell models. The most common modulated DEG were functionally annotated to the chemical metabolic process (e.g., CYP1A1, CYP1B1, and CYP1A2) and inflammatory response (e.g., EREG).

Indeed, some of the DEG common to all the cell models acutely or repeatedly exposed (i.e., *CYP1A1, CYP1A2* and *CYP1B1)*, and some other DEG specifically reported only in the cell models repeatedly exposed (i.e., *ALDH3A1* or *TIPARP)* are respectively canonical and less well-characterized aryl hydrocarbon receptor (AhR) target genes, and also in line with the relatively high contents of PAH within the UFP (Strapáčová et al. 2018). Le Vee et al. (2016) recently reported an AHR-dependent up-regulation of the heterodimeric amino acid transporter *LAT1* (*SLC7A5*)/*CD98hc* (*SLC3A2*) by diesel exhaust particle (DEP) extract, thereby supporting that DEP-derived PAH and other related compounds induced functional overexpression of amino acid transporter. In this work, *SLC7A5* was also among the DEG up-regulated in the cell models acutely or repeatedly exposed to the PAH-rich PUF under study. Moreover, Luo et al. (2018) demonstrated that IL-24 expression is highly induced by environmental AhR agonists, as well as PAH. IL-24 was among the main up-regulated DEG only found within the sensitive COPD-DHBE cell model acutely exposed to the PAH-rich PUF. Another DEG possibly up-regulated in all the cell models by AhR agonists is ENTPD8, through its hydrolase activity (Chari et al. 2007).

Other DEG reported in healthy and diseased cells acutely or rather repeatedly exposed to UFP are members of the epidermal growth factor (EGF) family, which are EGF-like ligands for the epidermal growth factor receptor (EGFR) and play a role in cell survival, proliferation and migration. Indeed, among the seven ligands bind to and activate EGFR, *EREG* and *EPGN*, which constitute low-affinity ligands, were up-regulated, with the highest FC found within sensible COPD-DHBE cells. EREG is shown to assist in the proliferation, repair, or regeneration (or a combination of these) (Bauer et al. 2017, Singh et al. 2016). EPGN, the most recently discovered EGFR ligand, is still understudied; however, NRF2 activation-induced *EPGN* upregulation under pathological conditions such as chronic inflammatory lung diseases (Riese and Cullum, 2014).

Besides all the above-mentioned DEG, found as deregulated in almost all the cell models under study, other DEG, as *FGF-1*, were only down-regulated in diseased and specially COPD-DHBE cells repeatedly exposed to UFP, thereby supporting their highest sensitivity. Simbori et al. (2016) underlined the importance of *FGF-1*, which notably participates in cell growth and differentiation, angiogenesis, and tissue repair, by reporting its ability to prevent lung to fibrosis and limit the progression of already established fibrosis by inhibiting TGF-β1-induced myofibroblast differentiation and downstream signaling pathways.

However, in this work, overexpression of *RAB37* could help to counteract the specific down-regulation of *FGF1* in asthma-DHBE cells repeatedly exposed to PUF. Indeed, RAB37 has been postulated as a tumor suppressive small GTPase for trafficking anti-tumor cargos. Cho et al. (2018) reported an uncharacterized mechanism by which RAB37 mediates exocytosis of secreted frizzled-related protein-1, an extracellular antagonist of WNT, to suppress WNT signaling and cancer stemness *in vitro* and *in vivo*.

In the opposite, in COPD-DHBE cells acutely and/or repeatedly exposed to PUF, several critical DEG (i.e., FGR, WNT7B, VIPR1 up-, and PPARGC1A down-regulation) could dramatically contribute to aggravate the repression of *FGF1*-downstream signaling pathways. Among the Src family kinases, well-known for their role in malignant transformation and tumor progression, as well as in signaling through cell surface integrins, FGR mediated outside-in signaling by β1 and β2 integrins, generally related to the immune complex-induced generation of an inflammatory response (Kovács et al. 2011; Mazzi et al. 2015). However, upon injury, surviving differentiated epithelial cells spread to maintain barrier function and recruit integrin-linked kinase to adhesion sites, which notably lead to WNT7B expression and secretion to further break quiescence, induce proliferation, and initiate epithelial repair (Volckaert et al. 2013, 2017). Both VIPR1 and VIPR2 help vasoactive intestinal peptide (VIP) to carry out its biological functions such as the regulation of airway mucus secretion, thereby suggesting their possible involvement in the pathogenesis of chronic bronchitis (Miotto et al. 2004). At least,

Lebleu et al. (2014) reported that invasive cancer cells used transcription co-activator, PPARGC1A, to increase mitochondrial biogenesis and respiration, also needed for proliferation, primary tumor growth or epithelial-to-mesenchymal program. According to Leclercq et al. (2018), the down-regulation of *PPARGC1A* specifically seen in COPD-DHBE cells repeatedly exposed to PUF could aggravate the mitochondrial dysfunction, frequently encountered in this diseased phenotype. Indeed, Lerner et al. (2016) have recently reported the critical role of mitochondria during inflammation, and better described how mitochondrial dysfunction contributes to the initiation and/or aggravation of chronic inflammatory pulmonary diseases, such as COPD.

Studying the transcriptomic profiles of normal human bronchial epithelial BEAS-2B cells exposed to FP, Zhou et al. (2016) and Longhin et al. (2016) reported the activation of some genes mainly involved in signaling pathways related to antioxidant response, xenobtiotic stimuli, metabolism, and inflammation and immunity, which might contribute to FP-related lung diseases. Besides, Grilli et al. (2018) showed that DEP induced the secretion of biomarkers associated to inflammation and transcription factors relevant for cardiovascular and lung diseases. By means of network reconstruction, they identified four genes (i.e., *STAT3, HIF1A, NFKB1, KRAS*) emerging as major regulators of transcriptional response of BEAS-2B cells to diesel exhaust.

Taken together, despite the non-negligeable inter-individual variability of the cell donors, the transcriptomic profiling by microarray technology we applied allowed identifying some new relevant signaling pathways, closely involved in the toxicity of acute or rather repeated exposure to FP and rather UFP. Moreover, the diseased cell models and notably COPD-DHBE cells showed a higher sensitivity. Accordingly, recent human studies supported the highest sensitivity of COPD outpatients towards air pollution-induced adverse health effects (Gao et al. 2019, Lee et al. 2019, Zhang et al. 2019). Interestingly, to our knowledge, this is the first work using relevant healthy and diseased 3D organo-typic mucocilary-phenotype models for better studying the toxicity of FP and UFP, their respective sensitivities towards FP or UFP, and the respective toxicities of FP or UFP collected at the same time in a similar urban surrounding.

However, future experiments will be required to limit the inter-individual variability between the cell donors of each cell phenotype, and, thereafter, to validate the activation of all the reported signaling pathways at the protein level. Although primary cells are regarded as the most physiologically relevant thanks to their closest resemblance to the native tissue in healthy and disease status, difficulties stemming from the isolation procedure and complex cultivation requirements, heterogeneity and high inter-donor variability and lastly their limited life span, still hinder their use for large scale experiments such as toxicant screening (Fizesan et al. 2018). Even though an *in vitro* model which would be able to respond to all questions of interests is still far from being

achieved, further improvements of the current models should fill the gap between *in vivo* and *in vitro* studies and further allow cheaper, ethically acceptable and high throughput toxicity evaluation (Feng et al. 2015).

CONCLUSION

Aiming to better evaluate and compare the underlying mechanisms closely involved in the toxicity of FP and UFP, on the one hand, and the sensitivity of healthy and diseased cell models, on the other hand, we have applied a relevant experimental strategy to acutely and repeatedly expose healthy and diseased 3D organotypic mucocilary-phenotype cells. By studying cytotoxic, inflammatory, epigenetic, and transcriptomic endpoints, we not only highlighted some trends to highest effects of UFP *versus* FP but also to highest sensitivity of asthma- and particularly COPD-DHBE *versus* NHBE cells. However, a further challenge will be to better characterize primary human airway epithelial cells and reduce the inter-individual variability between the cell donors. The use of innovative *in vitro* exposure systems as healthy and diseased 3D organo-typic mucocilary-phenotypes could yet be consider as a very useful and powerful promising tool in the field of the respiratory toxicology.

ACKNOWLEDGMENTS

The authors would like to thank Ms A. LOYENS from the “Microscopie électronique” platform (UMR-S 1172 - JPArc Centre de Recherche Jean-Pierre AUBERT Neurosciences et Cancer, Lille, France) for her skiful assistance for the microscopy observations, Dr M. TARDIVEL from the “Microscopie photonique, Imagerie cellulaire” platform (Faculté de médecine, Université de Lille, Lille, France) for her help for the confocal scanning microscopy observations, and Dr M. FIGEAC and his technical staff, from the “Génomique fonctionnelle et structurale” platform (Centre de Biologie et Pathologie, CHU Lille, Université de Lille) for the analysis of microrrays.

REFERENCES

Abbas I, Garçon G, Saint-Georges F, Billet S, Verdin A, Gosset P, Mulliez P, Shirali P. 2010. Occurrence of molecular abnormalities of cell cycle in L132 cells after *in vitro* short-term exposure to air pollution $PM_{2.5}$. Chem Biol Interact. 188, 558-565.

Abbas I, Verdin A, Escande F, Saint-Georges F, Cazier F, Mulliez P, Courcot D, Shirali P, Gosset P, Garçon G. 2016. In vitro short-term exposure to air pollution $PM_{2.5-0.3}$ induced cell cycle alterations and genetic instability in a human lung cell coculture model. Env Res. 147, 146-158.

Abbas I, Badran G, Verdin A, Ledoux F, Roumie M, Lo Guidice JM, Courcot D, Garçon G. 2019. In vitro evaluation of organic extractable matter from ambient $PM_{2.5}$ using human bronchial epithelial BEAS-2B cells: Cytotoxicity, oxidative stress, pro-inflammatory response, genotoxicity, and cell cycle deregulation. Environ Res. 171, 510-522.

Alleman LY, Lamaison L, Perdrix E, Robache A, Galloo JC. 2010. PM_{10} metal concentrations and source identification using positive matrix factorization and wind sectoring in a French industrial zone. Atmos Res. 96, 612-625.

Aoshiba K, Nagai A. 2004. Differences in airway remodeling between asthma and chronic obstructive pulmonary disease. Clin Rev Allergy Immunol. 27(1), 35-43.

Balharry D, Sexton K, BéruBé KA 2008. An in vitro approach to assess the toxicity of inhaled tobacco smoke components: nicotine, cadmium, formaldehyde and urethane. Toxicology. 244(1), 66-76.

Barnes PJ. 2009. The cytokine network in chronic obstructive pulmonary disease. Am J Respir Cell Mol Biol. 41(6): 631-638.

Barnes PJ. 2017. Cellular and molecular mechanisms of asthma and COPD. Clin Sci. 131(13), 1541-1558.

Bauer AK, Velmurugan K, Xiong KN, Alexander CM, Xiong J, Brooks R. 2017. Epiregulin is required for lung tumor promotion in a murine two-stage carcinogenesis model. Mol Carcinog. 56(1), 94-105.

Bérubé KA, Aufderheide M, Breheny D, Combes R, Duffin R, Clothier R, Forbes B, Marianna G, Gray A, Hall I, Kelly M, Lethem M, Liebsch M, Morello L, Morin JP, Seagrave JC, Schwartz M, Tetley T, Umachandran M. 2009. In vitro models of inhalation: toxicity and disease. J Altern Lab An. 37, 89-141.

Bérubé KA, Prytherch Z, Job C, Hughes T. 2010. Human primary bronchial lung cell constructs: the new respiratory models. Toxicology 278, 311-318.

Blasco H, Garçon G, Patin F, Veyrat-Durebex C, Boyer J, Devos D, Vourc'h P, Andres CR, Corcia P. 2017. Panel of oxidative stress and inflammatory biomarkers in ALS: a pilot study, Can J Neurol Sci 44(1), 90-95

Bocchi C, Bazzini C, Fontana F, Pinto G, Martino A, Cassoni F. 2016. Characterization of urban aerosol: seasonal variation of mutagenicity and genotoxicity of $PM_{2.5}$, PM_1 and semi-volatile organic compounds. Mutat. Res. Genet. Toxicol. Environ. Mutagen. 807, 16-23.

Boublil L, Assémat E, Borot MC, Boland S, Martinon L, Sciare J, Baeza-Squiban A. 2013. Development of a repeated exposure protocol of human bronchial epithelium in vitro to study the long-term effects of atmospheric particles. Toxicol in vitro 27, 533-542.

Burgel PR, Bourdin A, Chanez P, Chabot F, Chaouat A, Chinet T, deBlic J, Devillier P, Deschildre A, Didier A, 2011. Update on the roles of distal airways in COPD. Eur Respir Rev 20, 7-22.

Cantone L, Angelici L, Bollati V, Bonzini M, Apostoli P, Tripodi A, Bertazzi PA, Baccarelli AA. 2014. Extracellular histones mediate the effects of metal-rich air particles on blood coagulation. Environ Res. 132, 76-82.

Chari R, Lonergan KM, Ng RT, MacAulay C, Lam WL, Lam S. 2007. Effect of active smoking on the human bronchial epithelium transcriptome. BMC Genomics. 8, 297-305.

Chen X, Guan XJ, Luan CY, Guo XJ. 2015. Acetylation of lysine 9 on histone H3 is associated with increased pro-inflammatory cytokine release in a cigarette smoke-induced rat model through HDAC1 depression. Inflamm Res. 64:513-526.

Cho SH, Kuo IY, Lu PF, Tzeng HT, Lai WW, Su WC, Wang YC. 2018. Rab37 mediates exocytosis of secreted frizzled-related protein 1 to inhibit Wnt signaling and thus suppress lung cancer stemness. Cell Death Dis. 9(9), 868-878.

Crenn V, Fronval I, Petitprez D, Riffault V. 2017. Fine particles sampled at an urban background site and an industrialized coastal site in Northern France - Part 1: Seasonal variations and chemical characterization. Sci Total Environ. 578, 203-218.

Dergham M, Lepers C, Verdin A, Billet S, Cazier F, Courcot D, Shirali P, Garçon G. 2012. Prooxidant and proinflammatory potency of air pollution particulate matter ($PM_{0.3-2.5}$) produced in rural- urban- or industrial surroundings in human bronchial epithelial cells (BEAS-2B). Chem Res Toxicol. 25, 904-919.

Dergham M, Lepers C, Verdin A, Billet S, Cazier F, Courcot D, Shirali P, Garçon G. 2015. Temporal-spatial variations of the physicochemical characteristics of air pollution particulate matter ($PM_{0.3-2.5}$) and toxicological effects in human bronchial epithelial cells BEAS-2B. Env Res. 137, 256-267.

Ding R, Jin Y, Liu X, Ye H, Zhu Z, Zhang Y, Wang T, Xu Y. 2017. Dose- and time-effect responses of DNA methylation and histone H3K9 acetylation changes induced by traffic-related air pollution. Sci Rep. 3(7), 43737.

Feng W, Guo J, Huang H, Xia B, Liu H, Li J. 2015. Human normal bronchial epithelial cells: a novel *in vitro* cell model for toxicity evaluation. PLoS ONE 10 (4), 0123520.

Fizeşan I, Cambier S, Moschini E, Chary A, Pop A, Kiss B, Serchi T, Gutleb AC, Loghin F 2018. Review *in vitro* cellular models, a resourceful tool in respiratory toxicology. FARMACIA. 66 (4), 573-580.

Freishtat RJ, Watson AM, Benton AS, Iqbal SF, Pillai DK, Rose MC, Hoffman EP. 2011. Asthmatic airway epithelium is intrinsically inflammatory and mitotically dyssynchronous. Am J Respir Cell Mol Biol 44, 863-869.

Gao N, Li C, Ji J, Yang Y, Wang S, Tian X, Xu KF. 2019. Short-term effects of ambient air pollution on chronic obstructive pulmonary disease admissions in Beijing, China (2013-2017). Int J Chron Obstruct Pulmon Dis. 14, 297-309.

Garçon G, Dagher Z, Zerimech F, Ledoux F, Courcot D, Aboukais A, Puskaric E, Shirali P. 2006. Dunkerque city air pollution particulate matter-induced cytotoxicity oxidative stress and inflammation in human epithelial lung cells (L132) in culture. Toxicol in vitro. 20, 519-528.

Ghio AJ, Dailey LA, Soukup JM, Stonehuerner J, Richards JH, Devlin RB. 2013. Growth of human bronchial epithelial cells at an air-liquid interface alters the response to particle exposure. Part Fibre Toxicol 10, 25.

Grilli A, Bengalli R, Longhin E, Capasso L, Proverbio MC, Forcato M, Bicciato S, Gualtieri M, Battaglia C, Camatini M. 2018. Transcriptional profiling of human bronchial epithelial cell BEAS-2B exposed to diesel and biomass ultrafine particles. BMC Genomics. 19(1), 302.

Gualtieri M, Øvrevik J, Holme JA, Perrone MG, Bolzacchini E, Schwarze PE, Camatini M. 2010. Differences in cytotoxicity versus pro-inflammatory potency of different PM fractions in human epithelial lung cells. Toxicol in vitro 24, 29-39.

Gualtieri M, Ovrevik J, Mollerup S, Asare N, Longhin E, Dahlman HJ, Camatini M, Holme JA. 2011. Airborne urban particles (Milan winter-$PM_{2.5}$) cause mitotic arrest and cell death: Effects on DNA mitochondria AhR binding and spindle organization. Mutat Res. 713, 18-31.

Hackett TL, Singhera GK, Shaheen F, Hayden P, Jackson GR, Hegele RG, Van Eeden S, Bai TR, Dorscheid DR, Knight DA. 2011. Intrinsic phenotypic differences of asthmatic epithelium and its inflammatory responses to respiratory syncytial virus and air pollution. Am J Respir Cell Mol Biol. 45(5), 1090-1100.

Halonen JI, Lanki. T, Yli-Tuomi. T, Kulmala. M, Tiittanen. P, Pekkanen. J, 2008. Urban air pollution, and asthma and COPD hospital emergency room visits. Thorax 63(7), 635-641.

Holtzman M, Byers D, Alexander-Brett J, Wang X. 2014. The role of airway epithelial cells and innate immune cells in chronic respiratory disease. Nat Rev Immunol 14, 686-698.

Kesimer M, Kirkham S, Pickles RJ, Henderson AG, Alexis NE, Demaria G, Knight D, Thornton DJ, Sheehan JK. 2009. Tracheobronchial air-liquid interface cell culture: a model for innate mucosal defense of the upper airways? Am J Physiol Lung Cell Mol Physiol. 296, L92-L100.

Kovács M, Németh T, Jakus Z, Sitaru C, Simon E, Futosi K, Botz B, Helyes Z, Lowell CA, Mócsai A. 2014. The Src family kinases Hck, Fgr, and Lyn are critical for the generation of the in vivo inflammatory environment without a direct role in leukocyte recruitment. J Exp Med. 211(10), 1993-2011.

Kuleshov MV, Jones MR, Rouillard AD, Fernandez NF, Duan Q, Wang Z, Koplev S, Jenkins SL, Jagodnik KM, Lachmann A, McDermott MG, Monteiro CD, Gundersen GW, Ma'ayan A. 2016. Enrichr: a comprehensive gene set enrichment analysis web server 2016 update. Nucleic Acids Res. 44(W1): W90-W97.

LeBleu VS, O'Connell JT, Gonzalez Herrera KN, Wikman H, Pantel K, Haigis MC, de Carvalho FM, Damascena A, Domingos Chinen LT, Rocha RM, Asara JM, Kalluri R. 2014. PGC-1α mediates mitochondrial biogenesis and oxidative phosphorylation in cancer cells to promote metastasis. Nat Cell Biol. 16(10), 992-1003.

Leclercq B, Happillon M, Antherieu S, Hardy EM, Alleman LY, Grova N, Perdrix E, Appenzeller BM, Lo Guidice JM, Coddeville P, Garçon G. 2016. Differential responses of healthy and chronic obstructive pulmonary diseased human bronchial epithelial cells repeatedly exposed to air pollution-derived PM_4. Env Pollut. 218:1074-1088.

Leclercq B, Platel A, Antherieu S, Alleman LY, Hardy EM, Perdrix E, Grova N, Riffault V, Appenzeller BM, Happillon M, Neslany F, Coddeville P, Lo Guidice J-M, Garçon G. 2017. Genetic and epigenetic alterations in normal and sensitive COPD-diseased human bronchial epithelial cells repeatedly exposed to air pollution-derived $PM_{2,5}$. Env Pollut. 230, 163-177.

Leclercq B, Kluza J, Antherieu S, Sotty J, Alleman LY, Perdrix E, Loyens A, Coddeville P, Lo Guidice JM, Marchetti P, Garçon G. 2018. Air pollution-derived $PM_{2.5}$ impairs mitochondrial function in healthy and chronic obstructive pulmonary diseased human bronchial epithelial cells. Environ Pollut. 243, 1434-1449.

Lee J, Jung HM, Kim SK, Yoo KH, Jung KS, Lee SH, Rhee CK. (2019). Factors associated with chronic obstructive pulmonary disease exacerbation, based on big data analysis. Sci Rep. 9 (1), 6679.

Lerner CA, Sundar IK, Rahman I. 2016. Mitochondrial redox system dynamics and dysfunction in lung. Int J Biochem Cell Biol 81(Pt B), 294-306.

Le Vee M, Jouan E, Lecureur V, Fardel O. 2016. Aryl hydrocarbon receptor-dependent up-regulation of the heterodimeric amino acid transporter LAT1 (SLC7A5)/CD98hc (SLC3A2) by diesel exhaust particle extract in human bronchial epithelial cells. Toxicol Appl Pharmacol. 290, 74-85.

Lodovici M, Bigagli E. 2011. Oxidative stress and air pollution exposure. J Toxicol. 2011, 487074. doi:10.1155/2011/487074

Longhin E, Pezzolato E, Mantecca P, Holme JA, Franzetti A, Camatini M, Gualtieri M. 2013. Season linked responses to fine and quasi-ultrafine Milan PM in cultured cells. Toxicol in vitro 27, 551-559.

Longhin E, Capasso L, Battaglia C, Proverbio M,C, Consentino C, Cifola I, Mangano E, Camatini M, Gualtieri M. 2016. Integrative transcriptomic and protein analysis of human bronchial BEAS-2B exposed to seasonal urban particulate matter. Environ Poll. 209, 87-98.

Loxham M, Morgan-Walsh RJ, Cooper MJ, Blume C, Swindle EJ, Dennison PW, Howarth PH, Cassee FR, Teagle DAH, Palmer MR, Davies DE. 2015. The effects on bronchial epithelial mucociliary cultures of coarse fine and ultrafine particulate matter from an underground railway station, Toxicol Sci. 145(1), 98-107.

Luo YH, Kuo YC, Tsai MH, Ho CC, Tsai HT, Hsu CY, Chen YC, Lin P. 2017. Interleukin-24 as a target cytokine of environmental aryl hydrocarbon receptor agonist exposure in the lung. Toxicol Appl Pharmacol. 324, 1-11.

Mazzi P, Caveggion E, Lapinet-Vera JA, Lowell CA, Berton G. 2015. The Src-Family Kinases Hck and Fgr regulate early lipopolysaccharide-induced myeloid cell recruitment into the lung and their ability to secrete chemokines. J Immunol. 195(5), 2383-2395.

Mbengue S, Alleman LY, Flament P. 2014. Size-distributed metallic elements in submicronic and ultrafine atmospheric particles from urban and industrial areas in northern France. Atmospheric Res. 135-136, 35-47.

Mi H, Muruganujan A, Casagrande JT, Thomas PD. 2013. Large-scale gene function analysis with the PANTHER classification system. Nat Protoc. 8, 1551-1556.

Miotto D, Boschetto P, Bononi I, Zeni E, Cavallesco G, Fabbri LM, Mapp CE. 2004. Vasoactive intestinal peptide receptors in the airways of smokers with chronic bronchitis. Eur Respir J. 24(6), 958-963.

Oberdörster. G, Ferin. J, Lehner. B, 1994. Correlation between particle size, in vivo particle persistence, and lung injury. Environ Health Persp. 102, 173-179.

Peters A, Wichmann HE, Tuch T, Heinrich J, Heyder J. 1997. Respiratory effects are associated with the number of ultrafine particles. Am J Respir Crit Care Med. 155(4), 1376-1383.

Pillai DK, Sankoorikal BJV, Johnson E, Seneviratne AN, Zurko J, Brown KJ, Hathout Y, Rose MC. 2014. Directional secretomes reflect polarity-specific functions in an *in vitro* model of human bronchial epithelium. Am J Respir Cell Mol Biol. 50(2), 292-300.

Prytherch ZC, BéruBé KA. 2014. A normal and biotransforming model of the human bronchial epithelium for the toxicity testing of aerosols and solubilized substances. Altern Lab Anim. 42(6), 377-381.

Puchelle E, Zahm JM, Tournier JM, Coraux C. 2006. Airway epithelial repair, regeneration, and remodeling after injury in chronic obstructive pulmonary disease. ATS Journal 3(8), 726-733.

Recordati C, De Maglie M, Bianchessi S, Argentiere S, Cella C, Mattiello S, Cubadda F, Aureli F, D'Amato M, Raggi A, Lenardi C, Milani P, Scanziani E. 2016. Tissue distribution and acute toxicity of silver after single intravenous administration in mice: nano-specific and size-dependent effect. Part Fibre Toxicol. 13(12).

Riese DJ 2nd, Cullum RL. 2014. Epiregulin: roles in normal physiology and cancer. Semin Cell Dev Biol. 28, 49-56.

Ritchie ME, Phipson B, Wu D, Hu Y, Law CW, Shi W, Smyth GK. 2015. Limma powers differential expression analyses for RNA-sequencing and microarray studies. Nucleic acids Res. 43(7), e47.

Saleh Y, Antherieu S, Dusautoir R, Alleman LY, Sotty J., De Sousa C, Platel A., Perdrix E, Riffault V., Fronval I., Nesslany F., Canivet L, Garçon G., Lo Guidice JM. 2019. Exposure to atmospheric ultrafine particles induces severe lung inflammatory response and tissue remodeling in mice. Int J Environ Res Public health. 4, 16(7).

Schuliga M. 2015. NF-kappa B signaling in chronic inflammatory airway disease, Biomolecules 5, 1266-1283.

Shimbori C, Bellaye PS, Xia J, Gauldie J, Ask K, Ramos C, Becerril C, Pardo A, Selman M, Kolb M. 2016. Fibroblast growth factor-1 attenuates TGF-β1-induced lung fibrosis. J Pathol. 240(2), 197-210.

Singh B, Carpenter G, Coffey RJ. 2016. EGF receptor ligands: recent advances. F1000Res. 8, 5. doi:10.12688/f1000research.9025.1.

Strapáčová S, Brenerová P, Krčmář P, Andersson P, van Ede KI, van Duursen MBM, van den Berg M, Vondráček J, Machala M. 2018. Relative effective potencies of dioxin-like compounds in rodent and human lung cell models. Toxicology. 404-405, 33-41.

To T, Zhu J, Larsen K, Simatovic J, Feldman L, Ryckman K, Gershon A, Lougheed MD, Licskai C, Chen H, Villeneuve PJ, Crighton E, Su Y, Sadatsafavi M, Williams D, Carlsten C. 2016. Canadian Respiratory Research Network, 2016. Progression from asthma to chronic obstructive pulmonary disease, COPD; is air pollution a risk factor? Am J Respir Crit Care Med. 194(4), 429-438.

Vales G, Rubio L, Marcos R. 2015. Long-term exposures to low doses of titanium dioxide nanoparticles induce cell transformation but not genotoxic damage in BEAS-2B cells. Nanotoxicology 9, 568-578.

Volckaert T, Campbell A, De Langhe S. 2013. c-Myc regulates proliferation and Fgf10 expression in airway smooth muscle after airway epithelial injury in mouse. PLoS One. 8(8), 71426.

Volckaert T, Yuan T, Chao CM, Bell H, Sitaula A, Szimmtenings L, El Agha E, Chanda D, Majka S, Bellusci S, Thannickal VJ, Fässler R, De Langhe SP. 2017. Fgf10-Hippo epithelial-mesenchymal crosstalk maintains and recruits lung basal stem cells. Dev Cell. 43(1), 48-59.

Wang T, Garcia JGN, Zhang W. 2012. Epigenetic regulation in particulate matter-mediated cardiopulmonary toxicities: a systems biology perspective. Curr Pharmacogenomics Person Med. 10(4), 314-321.

World Health Organization, 2016. 7 million premature deaths annually linked to air pollution. Available at www.who.int/mediacentre/news/releases/2014/air-pollution/en/ (March 24, 2019).

Zhang Z, Wang J, Liu F, Yuan L, Yuan J, Chen L, Zhong N, Lu W. 2019. Impacts of event-specific air quality improvements on total hospital admissions and reduced systemic inflammation in COPD patients. PLoS One. 14(3), 0208687.

Zhou W, Tian D, He J, Wang Y, Zhang L, Cui L, Jia L, Li L, Shu Y, Yu S. 2016. Repeated $PM_{2,5}$ exposure inhibits BEAS-2B cell P53 expression through ROS-Akt-DNMT3B pathway-mediated promoter hypermethylation, Oncotarget 7, 20691-20703.

Zhou W, Tian D, He J, Zhang L, Tang X, Zhang L, Wang Y, Li L, Zhao J, Yuan X, Peng S. 2017. Exposure scenario: Another important factor determining the toxic effects of $PM_{2,5}$ and possible mechanisms involved. Env Pollut. 226, 412-425.

FIGURE LEGENDS

Figure 1: Observations with a Zeiss Axio Vert.A1 photonic microscope (magnitude x 1000) of chronic obstructive pulmonary disease (COPD) diseased human bronchial epithelial (DHBE) cells cultivated in immerged conditions until confluency (Figure 1A) and after 28 days of differentiation at the air-liquid interface culture conditions (Figure 1B). Observations with a Zeiss EM900 transmission electronic microscope (magnitude x 20,000) of COPD-DHBE cells after 28-days of differentiation (Figure 1C). Observations with a Zeiss confocal scanning microscope LSM 710 (magnitude x 5,000) of pan cytokeratin, mucin-5ac (MUC5AC), and zonula occludens-1 (ZO-1) immunostaining of COPD-DHBE cells (Figures 1D, 1E, and 1F, respectively). Nuclei are revealed in blue with DAPI.

Figure 2: Normal human bronchial epithelial (NHBE), and asthma- and chronic obstructive pulmonary disease (COPD)-diseased human bronchial epithelial (DHBE) cells were grown and thereafter differentiated for 28 days at the air-liquid interface. ATP concentrations (RLU) in cells and glucose-6-phoshate dehydrogenase (G6PD) activity (RFU) in cell-free culture media were measured immediately after one (Figures 2A and 2C) or three (Figures 2B and 2D) 6 h exposures with 18 h intervals to FP or UFP at the dose of 5 µg/cm². Values are depicted as means and standard deviations (n = 4). (Non-parametric test of Kruskal Wallis with a post hoc test of Dunn's for multiple comparison correction; versus NHBE, asthma- or COPD-DHBE controls: *: $p < 0.05$).

Figure 3: Tumor necrosis factor-alpha (TNFα), interleukine-1 beta (IL-1β), interleukine-6 (IL-6), interleukine-8 (IL-8), granulocyte macrophage-colony stimulating factor (GM-CSF), monocyte chemoattractant protein 1 (MCP-1), regulated upon activation normal T cell expressed (RANTES), and transforming growth factor-alpha, TGFα) concentrations (pg/mL) determined in cell-free culture media of control normal human bronchial epithelial (NHBE), and asthma- and chronic obstructive pulmonary disease (COPD)-diseased human bronchial epithelial (DHBE) cells, grown and thereafter differentiated for 28 days at the air-liquid interface. Values are depicted as means and standard deviations (n = 4). (Non-parametric test of Kruskal Wallis with a post hoc test of Dunn's for multiple comparison correction; versus NHBE controls).

Figure 4: Tumor necrosis factor-alpha (TNFα), interleukine-1 beta (IL-1β), interleukine-6 (IL-6), and interleukine-8 (IL-8) concentrations (pg/mL) determined in cell-free culture media of normal human bronchial

epithelial (NHBE), and asthma- and chronic obstructive pulmonary disease (COPD)-diseased human bronchial epithelial (DHBE) cells, grown and thereafter differentiated for 28 days at the air-liquid interface, and after one (Figures 4A, 4C, 4E, and 4G) or three (Figures 4A, 4C, 4E, and 4G) 6 h exposures with 18 h intervals to FP or UFP at the dose of 5 µg/cm². Values are depicted as means and standard deviations (n = 4). (Non-parametric test of Kruskal Wallis with a post hoc test of Dunn's for multiple comparison correction; versus NHBE, asthma- or COPD-DHBE controls: *: $p < 0.05$).

Figure 5: Granulocyte macrophage-colony stimulating factor (GM-CSF), monocyte chemoattractant protein 1 (MCP-1), regulated upon activation normal T cell expressed (RANTES), and transforming growth factor-alpha, TGFα) concentrations (pg/mL) determined in cell-free culture media of normal human bronchial epithelial (NHBE), and asthma- and chronic obstructive pulmonary disease (COPD)-diseased human bronchial epithelial (DHBE) cells, grown and thereafter differentiated for 28 days at the air-liquid interface, and after one (Figures 5A, 5C, 5E, and 5G) or three (Figures 5A, 5C, 5E, and 5G) 6 h exposures with 18 h intervals to FP or UFP at the dose of 5 µg/cm². Values are depicted as means and standard deviations (n = 4). (Non-parametric test of Kruskal Wallis with a post hoc test of Dunn's for multiple comparison correction; versus NHBE, asthma- or COPD-DHBE controls: *: $p < 0.05$).

Figure 6: Histone acetyltransferase (HAT) and deacetylase (HDAC) activities (RFU) determined in normal human bronchial epithelial (NHBE), and asthma- and chronic obstructive pulmonary disease (COPD)-diseased human bronchial epithelial (DHBE) cells, grown and thereafter differentiated for 28 days at the air-liquid interface, and after one (Figures 6A and 6C) or three (Figures 6B and 6D) 6 h exposures with 18 h intervals to FP or UFP at the dose of 5 µg/cm². Values are depicted as means and standard deviations (n = 4). H3K9 histone acetylation (H3k9ac) determined in NHBE, and asthma- and COPD-DHBE cells, grown and thereafter differentiated for 28 days at the air-liquid interface, and after one (Figures 6E and 6G) or three (Figures 6F and 6H) 6 h exposures with 24 h intervals to FP or UFP at the dose of 5 µg/cm². Total H3 histone was used as standard control to study H3 histone acetylation. Values are presented as H3K9/H3 expression ratio, and results have been normalized to controls. Mean ± standard mean of error (SEM). (Non-parametric test of Kruskal Wallis with a post hoc test of Dunn's for multiple comparison correction; versus NHBE, asthma- or COPD-DHBE controls: *: $p < 0.05$).

Figure 7: Venn diagram representing the changes of gene expression in normal human bronchial epithelial (NHBE), and asthma- and chronic obstructive pulmonary disease (COPD)-diseased human bronchial epithelial (DHBE) cells, grown and thereafter differentiated for 28 days at the air-liquid interface, and after one (Figure 7A) or three (Figure 7B) 6 h exposures with 18 h intervals to UFP at the dose of 5 µg/cm². Linear models for microarray data package version 3.22.7 using the moderated t statistics with normalized data was used (n = 4). Differentially expressed genes were reported with a raw p value < 0.01 and absolute fold change > 1.5.

Figure 8: Biological processes and molecular functions triggered in normal human bronchial epithelial (NHBE), and asthma- and chronic obstructive pulmonary disease (COPD)-diseased human bronchial epithelial (DHBE) cells, grown and thereafter differentiated for 28 days at the air-liquid interface, and after one (Figure 8A) or three (Figure 8B) 6 h exposures with 18 h intervals to UFP at the dose of 5 µg/cm². Gene function analysis was done by using the PANTHER classification system, version 13.1 based on the gene ontology consortium database. Gene ontology classification of genes differentially expressed between PUF treated and untreated samples. The functions of genes identified cover two main categories: biological process and molecular function. The left y axe indicates the number of genes in a category. Enrichment analysis was performed with the freely available web-based tool Enrichr (http://amp.pharm.mssm.edu/Enrichr) to identify statistically deregulated pathways on the basis of Kyoto Encyclopedia of Genes and Genomes database (Fisher exact test, adj p value < 0.05). The gene interaction networks were generated through the use of Ingenuity pathway analysis (IPA, QIAGEN Inc., https://www.qiagenbioinformatics.com/products/ingenuity-pathway-analysis).

Figure S1: Particles surface content in FP or UFP, as investigated by X-Ray photoelectron spectroscopy. Analyses have been carried out using monochromatic source MgKα which spot size can be adjust from 400 µm to 30 µm diameter. Samples were setting up on silicon wafer, introduced in primary vacuum chamber (10^{-7} mbar, 60 min) to degas and transferred in analysis chamber (10^{-9} mbar, 320 min).

FIGURE 1

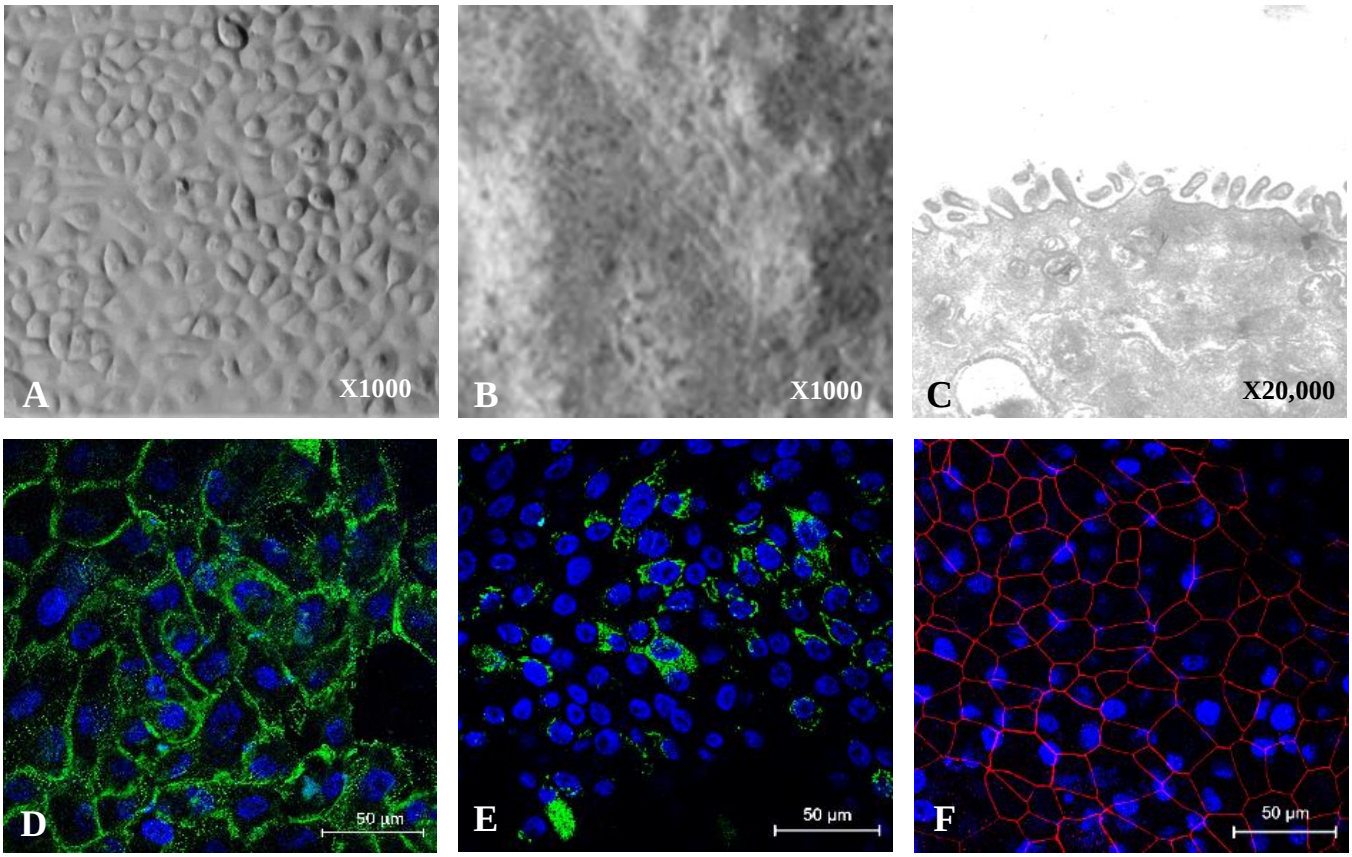

FIGURE 2

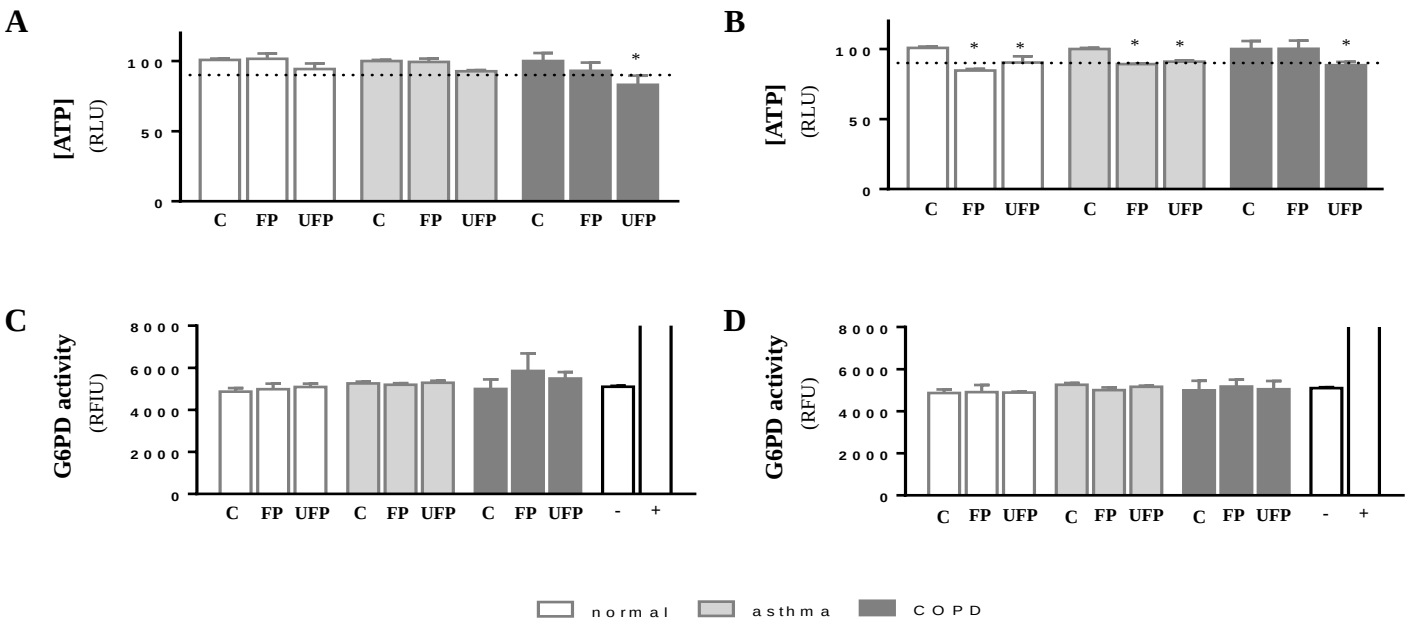
A
[ATP]
(RLU)
100
50
0
C FP UFP C FP UFP C FP UFP
*
B
[ATP]
(RLU)
100
50
0
C FP UFP C FP UFP C FP UFP
*
C
G6PD activity
(RFIU)
8000
6000
4000
2000
0
C FP UFP C FP UFP C FP UFP - +
D
G6PD activity
(RFU)
8000
6000
4000
2000
0
C FP UFP C FP UFP C FP UFP - +
normal
asthma
COPD

FIGURE 3

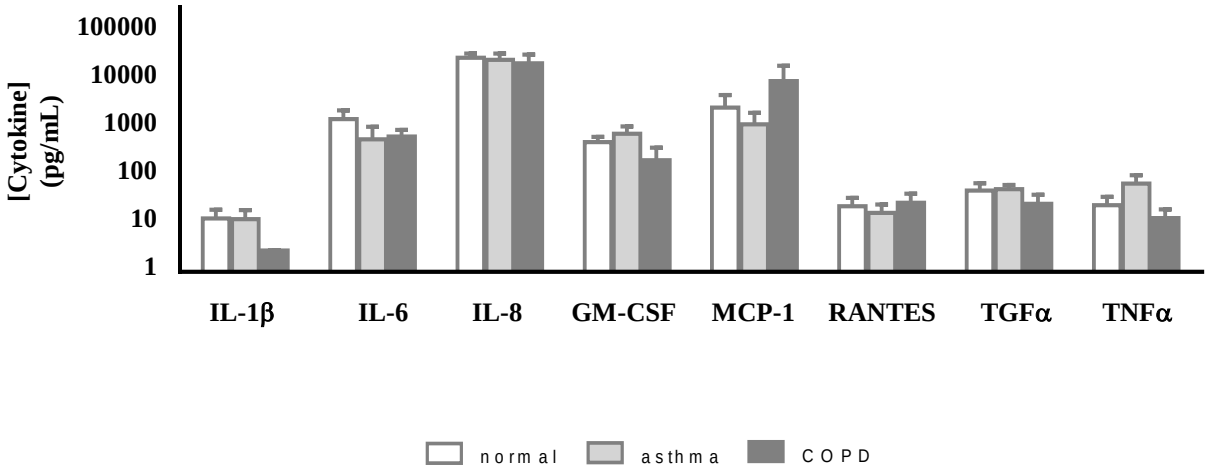
[Cytokine] (pg/mL)
100000
10000
1000
100
10
1
IL-1β
IL-6
IL-8
GM-CSF
MCP-1
RANTES
TGFα
TNFα
normal
asthma
COPD

FIGURE 4

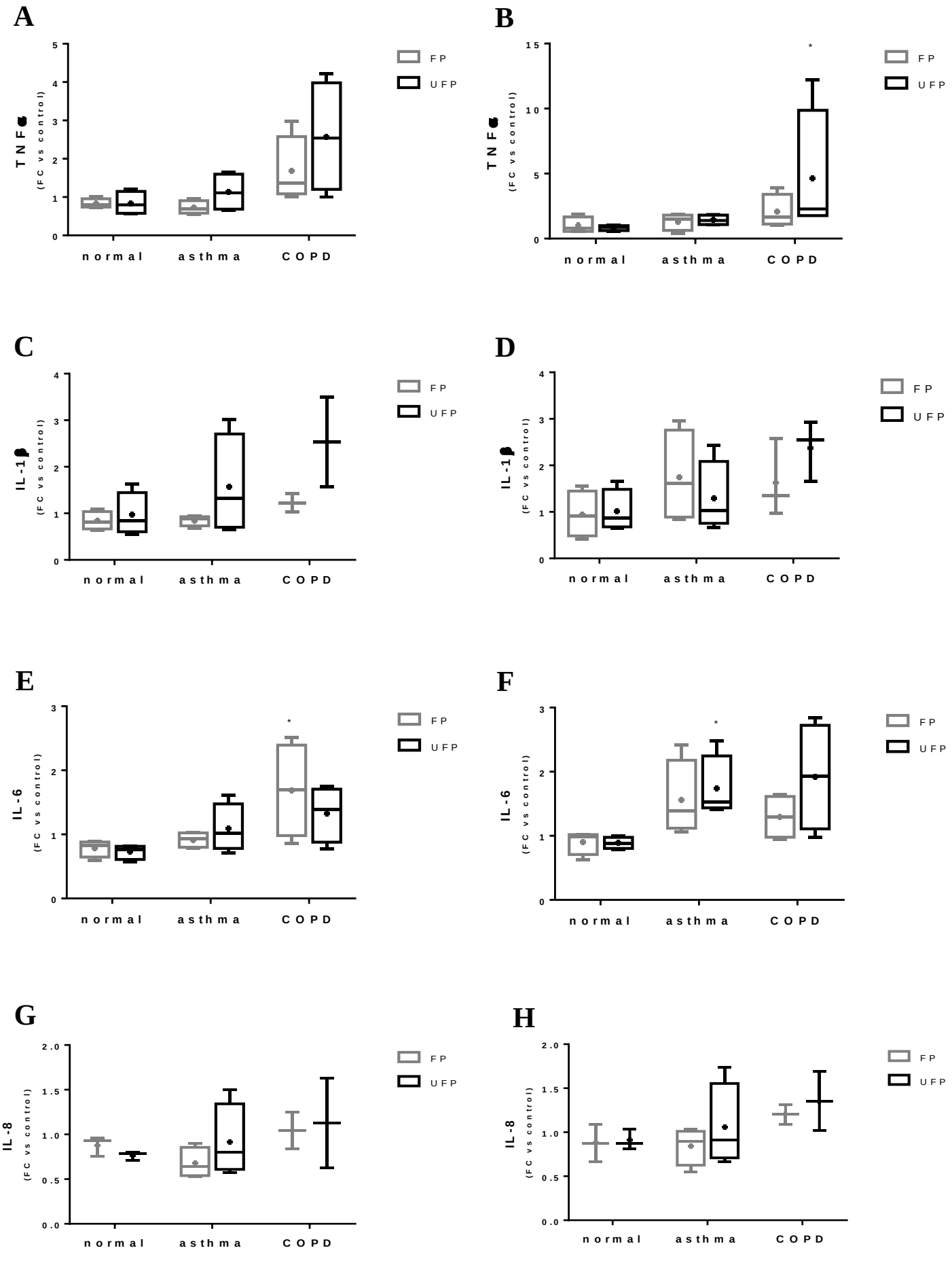
A
B
C
D
E
F
G
H
TNFα
IL-1β
IL-6
IL-8
(FC vs control)
FP
UFP
normal
asthma
COPD
*

FIGURE 5

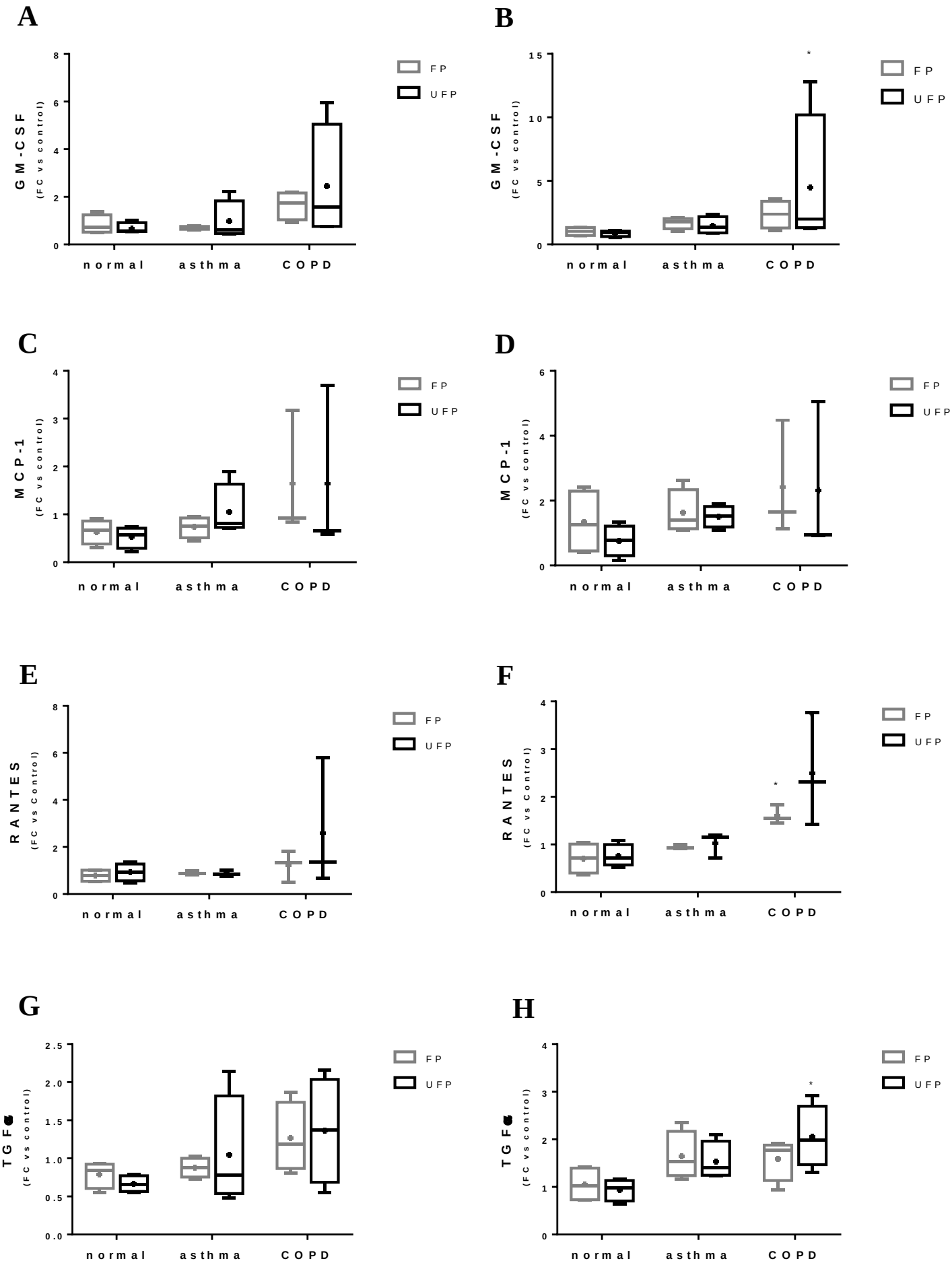
A
B
C
D
E
F
G
H
GM-CSF
(FC vs control)
MCP-1
(FC vs control)
RANTES
(FC vs Control)
TGFβ
(FC vs control)
FP
UFP
normal
asthma
COPD

FIGURE 6

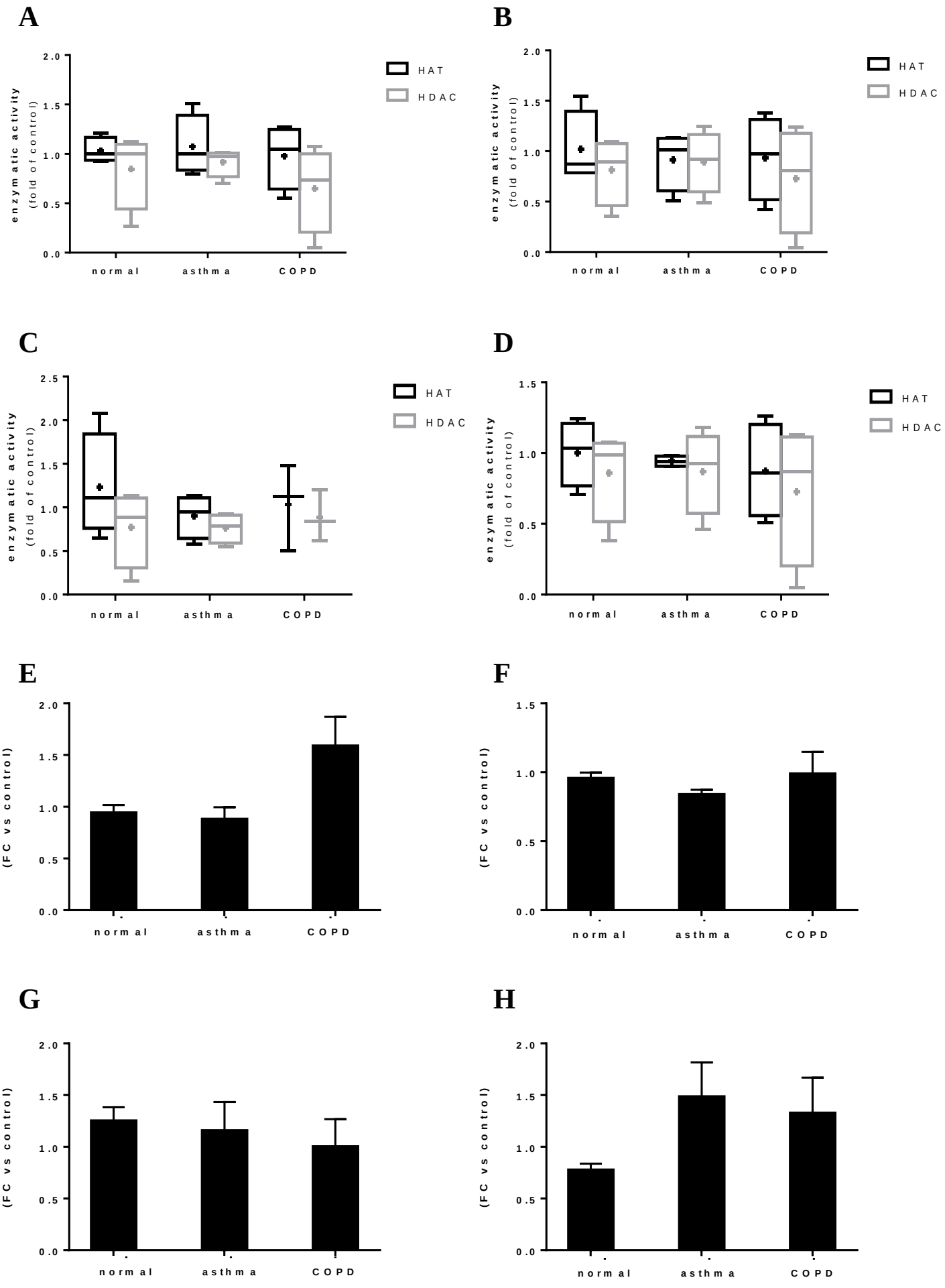
A
B
C
D
E
F
G
H
HAT
HDAC
enzymatic activity
(fold of control)
(FC vs control)
normal
asthma
COPD

FIGURE 7

A

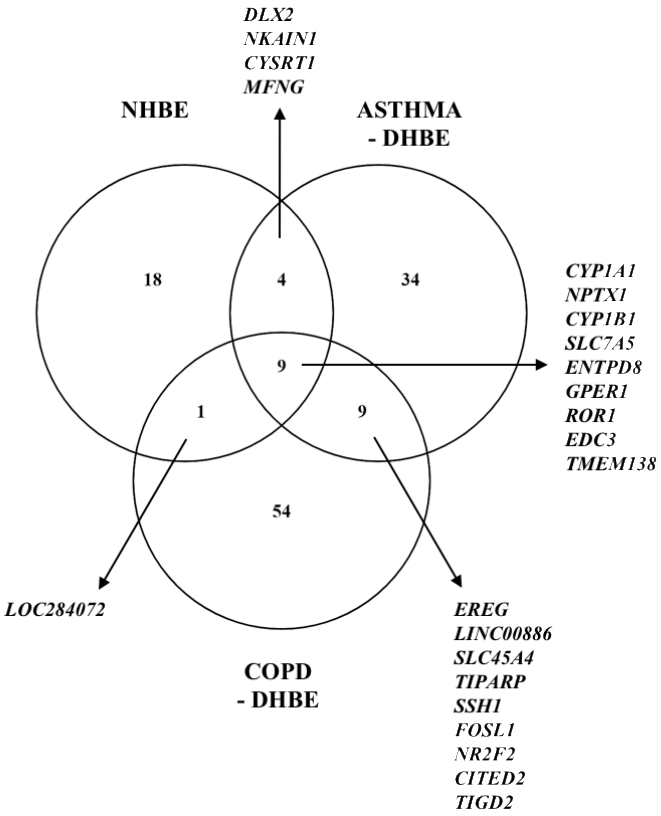
DLX2
NKAIN1
CYSRT1
MFNG
NHBE
ASTHMA
- DHBE
18
4
34
CYP1A1
NPTX1
CYP1B1
SLC7A5
ENTPD8
GPER1
ROR1
EDC3
TMEM138
9
1
9
54
LOC284072
EREG
LINC00886
SLC45A4
TIPARP
SSH1
FOSL1
NR2F2
CITED2
TIGD2
COPD
- DHBE

B

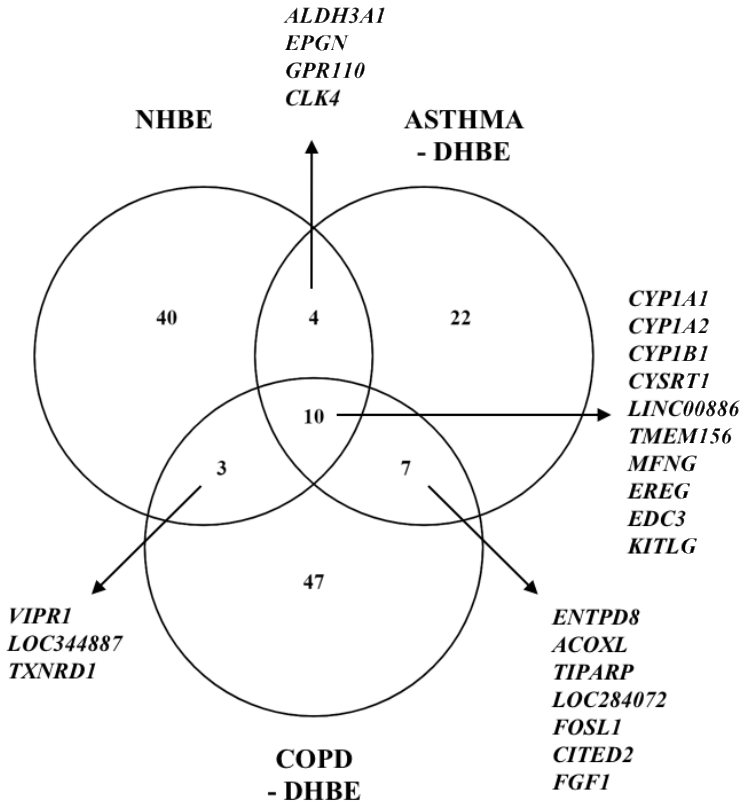
ALDH3A1
EPGN
GPR110
CLK4
NHBE
ASTHMA
- DHBE
40
4
22
CYP1A1
CYP1A2
CYP1B1
CYSRT1
LINC00886
TMEM156
MFNG
EREG
EDC3
KITLG
10
3
7
47
VIPR1
LOC344887
TXNRD1
ENTPD8
ACOXL
TIPARP
LOC284072
FOSL1
CITED2
FGF1
COPD
- DHBE

FIGURE 8

A

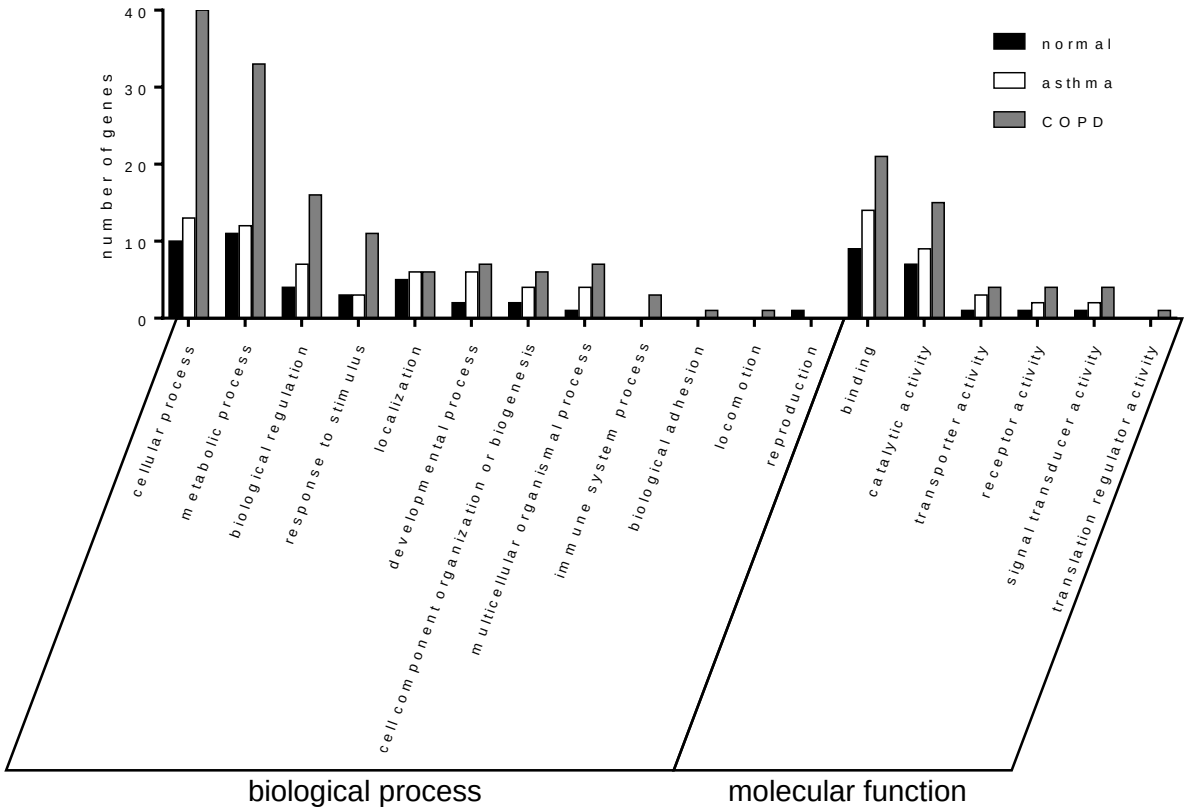
number of genes
40
30
20
10
0
normal
asthma
COPD
cellular process
metabolic process
biological regulation
response to stimulus
localization
developmental process
cell component organization or biogenesis
multicellular organismal process
immune system process
biological adhesion
locomotion
reproduction
binding
catalytic activity
transporter activity
receptor activity
signal transducer activity
translation regulator activity
biological process
molecular function

B

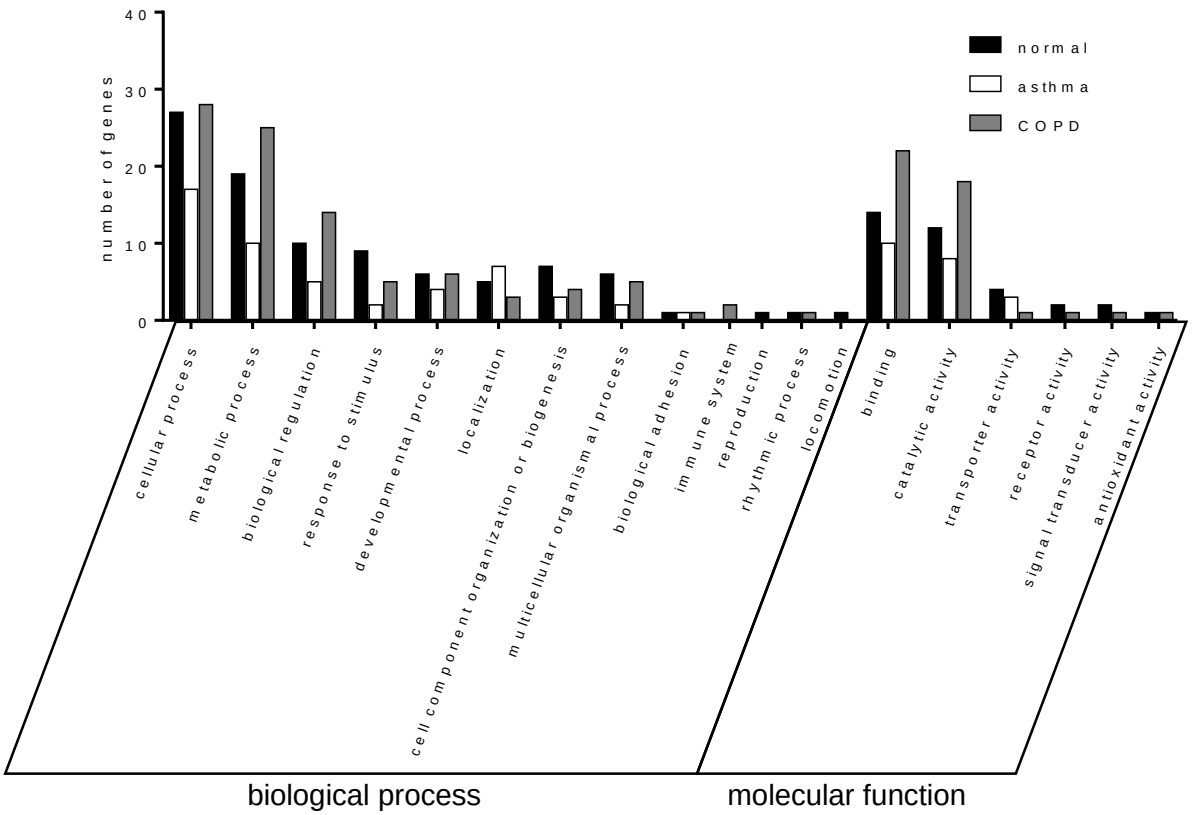
number of genes
40
30
20
10
0
normal
asthma
COPD
cellular process
metabolic process
biological regulation
response to stimulus
developmental process
localization
cell component organization or biogenesis
multicellular organismal process
biological adhesion
immune system
reproduction
rhythmic process
locomotion
binding
catalytic activity
transporter activity
receptor activity
signal transducer activity
antioxidant activity
biological process
molecular function

Table 1: Elemental concentrations in FP and UFP

Element (µg/g)	FP	UFP
As	23.0	64.8
Ba	140.3	64.4
Be	0.4	0.3
Cd	16.9	19.3
Ce	8.5	6.3
Co	5.4	9.3
Cs	4.4	8.9
Cu	367.0	425.2
La	8.4	3.1
Mn	1350.4	582.2
Mo	25.6	36.7
Ni	98.7	199.7
Pb	399.4	541.9
Rb	26.3	44.1
Sb	47.1	49.3
Sn	49.6	111.1
Sr	91.8	49.3
Ti	3.0	5.7
Zn	4000.2	2460.7
Cr	97.3	120.7
V	75.0	196.3
Al	5252.2	3621.1
Ca	17,904.5	11,857.4
Fe	16,406.1	10,267.0
K	1240.3	#
Mg	6591.3	#
Na	43,510.8	#
Si	9383.5	7568.1

Values not considered in the analysis due to their high amount in HBSS.

Table 2: PAH concentrations in FP and UFP

PAH (µg/g) [a]	FP	UFP
FLA	5.1	4.3
PYR	4.2	3.7
BcPHE	0.4	0.2
BaA	6.9	4.2
CHR	6.8	2.8
5MCHR	1.1	3.4
BeP	9.9	0.8
BbF	7.6	8.0
BjF	4.7	9.9
BkF	7.4	4.6
BaP	3.8	5.3
DalP	0.8	0.4
DahA	2.6	1.5
BghiP	12.0	12.5
IP	14.0	12.1
DaeP	3.6	2.7
ANTH	0.1	3.3
COR	2.9	4.5

[a] Fluoranthene (FLA), Pyrene (PYR), Benzo(c)phenanthrene (BcDE), Benzo(a)anthracene (B(a)A), Chrysene (CHR), 5-Methylchrysene (5-MCHR), Benzo(e)pyrene (BeP), Benzo(b)fluoranthene (BbF), Benzo(j)fluoranthene (BjF), Benzo(k)fluoranthene (BkF), Benzo(a)pyrene (BaP), Dibenzo(a,l)pyrene (Da,lP), Dibenzo(a,h)anthracene (Da,hA), Benzo(g,h,i)perylene (Bg,h,iPe), Indeno(1,2,3-c,d)pyrene (I-1,2,3-c,dP, Dibenzo(a,e)pyrene (Da,eP), Anthanthrene (ANTH), and Coronene (COR)

Table 3: Top 30 list of the differentially expressed genes in NHBE cells acutely or repeatedly exposed to UFP

Acute exposure			Repeated exposures		
Gene symbol	**Fold change**	***p* value**	**Gene symbol**	**Fold change**	***p* value**
CYP1A1	32.11	1.08E-06	*CYP1A1*	34.22	7.58E-07
NPTX1	10.97	8.23E-04	*ALDH3A1*	11.51	1.65E-03
CYP1B1	6.31	8.69E-07	*CYP1A2*	7.65	1.20E-04
SLC7A5	4.77	3.08E-04	*CYP1B1*	5.88	1.85E-08
ENTPD8	4.66	1.71E-03	*EPGN*	5.24	3.49E-03
GPER1	4.29	8.84E-04	*MYZAP*	4.38	4.03E-04
ROR1	4.23	9.02E-04	*VIPR1*	4.31	3.83E-03
DLX2	3.85	2.74E-04	*BCAS2*	4.22	4.45E-03
NKAIN1	3.38	2.94E-03	*LOC344887*	3.81	3.95E-03
COX10	3.11	6.26E-03	*NQO1*	3.59	7.30E-03
CYSRT1	3.09	8.37E-04	*ARHGEF2*	3.24	4.14E-03
MFNG	2.40	2.77E-03	*CRHR1-IT1*	3.20	4.36E-03
LOC284072	2.30	4.78E-03	*CYSRT1*	3.18	4.78E-04
ZNF799	2.11	2.66E-03	*GPR110*	2.90	8.75E-03
ATF6B	2.10	3.39E-03	*RBM23*	2.72	5.23E-03
KCTD18	1.90	9.88E-04	*LINC00886*	2.69	1.43E-03
SRR	1.87	4.98E-04	*C11orf91*	2.60	3.17E-03
EDC3	1.86	1.28E-03	*TMEM156*	2.50	6.21E-04
LINC00673	1.77	9.22E-03	*DHX30*	2.44	4.66E-03
PHTF1	1.76	7.12E-03	*MFNG*	2.43	2.42E-03
TMEM64	-1.68	4.27E-03	*FAM120C*	-1.98	7.61E-03
LOC100131831	-1.91	9.34E-03	*KITLG*	-2.02	4.44E-03
TET2	-2.06	5.45E-03	*LOC100131831*	-2.02	4.82E-03
ZNF552	-2.19	1.00E-03	*GPR155*	-2.06	6.74E-03
BMP2K	-2.24	5.58E-03	*PER2*	-2.16	2.33E-03
NHLRC3	-2.43	9.78E-03	*LRIG3*	-2.36	4.00E-03
KCTD19	-2.44	6.55E-03	*lnc-CRISP2-1*	-2.43	1.52E-03
LOC100507520	-2.58	7.77E-03	*C2orf50*	-2.48	9.54E-03
HLA-DOA	-2.85	7.18E-03	*BOLA3-AS1*	-3.60	8.80E-03
			SLC1A3	-4.89	1.01E-05

Table 4: Top 30 list of the differentially differentially expressed genes in asthma-DHBE cells acutely or repeatedly exposed to UFP

Acute exposure			Repeated exposures		
Gene symbol	**Fold change**	***p* value**	**Gene symbol**	**Fold change**	***p* value**
CYP1A1	27.54	9.77E-07	*CYP1A1*	26.49	4.67E-08
NPTX1	11.38	3.92E-04	*ALDH3A1*	6.75	1.23E-06
ENTPD8	7.48	3.44E-05	*SLC16A6*	5.59	3.07E-06
EPGN	6.12	9.18E-04	*RAB37*	5.25	1.00E-04
F2RL3	5.76	3.02E-03	*CYP1B1*	5.15	3.24E-04
SLC16A6	5.56	8.16E-04	*ENTPD8*	4.90	7.31E-04
CYP1B1	5.41	1.77E-06	*UNC13C*	4.81	7.83E-04
NKAIN1	4.88	8.64E-05	*EPGN*	4.80	8.63E-04
UNC13C	4.81	6.22E-03	*CYP1A2*	4.13	9.27E-04
STC2	4.52	5.43E-03	*XLOC_l2_11627*	3.60	9.82E-04
SLC7A5	4.13	5.24E-04	*LINC00880*	3.51	1.18E-03
CHDH	3.93	9.14E-03	*SLC7A5*	3.25	1.43E-03
GPER1	3.76	1.04E-03	*LINC00886*	3.24	1.86E-03
XLOC_l2_11627	3.74	6.75E-04	*GPR110*	3.02	2.17E-03
LOC100128317	3.47	4.29E-03	*EREG*	2.80	3.23E-03
ROR1	3.03	6.19E-03	*CYSRT1*	2.72	3.35E-03
DLX2	2.95	1.74E-03	*ACOXL*	2.45	3.53E-03
LINC00880	2.84	5.35E-03	*MFNG*	2.35	3.63E-03
FAM167A	2.83	3.03E-03	*TIPARP*	2.22	3.91E-03
RPS6KA5	2.66	6.71E-03	*lnc-SLC44A5-4*	2.22	3.93E-03
TRPS1	-1.55	5.98E-03	*FAM46A*	-1.71	8.41E-03
CITED2	-1.57	1.98E-03	*SERTAD4*	-1.78	8.59E-03
HERC2	-1.57	8.80E-03	*PDE5A*	-1.78	8.66E-03
TIGD2	-1.62	1.11E-04	*ALDH1B1*	-1.80	8.84E-03
RIN2	-1.70	1.89E-03	*ATP1A1-AS1*	-1.87	8.88E-03
TRAK1	-2.08	4.99E-03	*KITLG*	-1.95	9.41E-03
lnc-C16orf55-1	-2.30	8.34E-03	*HEY1*	-2.29	9.64E-03
SERTAD4	-2.32	2.16E-04	*CTGF*	-2.66	9.73E-03
FAM84A	-2.45	3.30E-03	*FGF1*	-4.78	9.87E-03
CASC10	-2.83	2.00E-03	*CNIH3*	-5.03	9.92E-03

Table 5: Top 30 list of the differentially expressed genes in COPD-DHBE cells acutely or repeatedly exposed to UFP

Acute exposure			Repeated exposures		
Gene symbol	**Fold change**	**p value**	**Gene symbol**	**Fold change**	**p value**
CYP1A1	98.13	1.91E-09	*CYP1A1*	103.02	1.45E-09
IL24	7.88	2.53E-09	*CYP1B1*	7.32	2.53E-09
NPTX1	7.84	1.46E-07	*ZNF644*	7.15	1.76E-07
CYP1B1	7.44	3.42E-06	*CYP1A2*	6.31	3.54E-05
C5AR2	6.42	1.47E-04	*SCL45A4*	5.15	1.35E-04
CYP1A2	5.41	2.31E-04	*ENTPD8*	4.72	3.39E-04
ENTPD8	4.74	2.48E-04	*SNHG11*	4.14	3.45E-04
VIPR1	4.59	3.30E-04	*VIPR1*	4.03	3.81E-04
E2F7	4.53	4.88E-04	*FGR*	3.64	4.21E-04
SLC7A5	4.24	5.76E-04	*EREG*	3.24	4.64E-04
WNT7B	4.12	6.06E-04	*WNT7B*	3.22	5.10E-04
ROR1	4.01	6.28E-04	*ACOXL*	3.14	8.07E-04
HILS1	3.82	7.51E-04	*LOC344887*	3.04	1.02E-03
GPER1	3.40	9.23E-04	*LOC284072*	2.85	1.06E-03
DEF6	3.34	9.76E-04	*LINC00886*	2.73	1.10E-03
FGR	3.12	1.05E-03	*C2CD3*	2.72	1.10E-03
LOC284072	3.12	1.09E-03	*TIPARP*	2.50	1.12E-03
ACOXL	3.10	1.23E-03	*CYSRT1*	2.50	1.21E-03
GPR157	2.93	1.54E-03	*ANKRD42*	2.45	1.25E-03
lnc-SLC15A4-12	2.87	1.57E-03	*lnc-GPR55-2*	2.43	1.59E-03
TIGD2	-1.40	8.23E-03	*KITLG*	-2.05	8.36E-03
CITED2	-1.59	8.45E-03	*ID3*	-2.11	8.58E-03
NR2F2	-1.59	8.50E-03	*LINC00313*	-2.22	8.76E-03
lnc-DNAI1-1	-1.87	8.82E-03	*lnc-DMRT2-1*	-2.38	8.81E-03
ZDHHC8	-1.87	8.83E-03	*FAM171A2*	-2.71	8.83E-03
SUMO2	-2.04	9.01E-03	*SENCR*	-2.75	8.91E-03
FAM13A	-2.21	9.10E-03	*LFNG*	-3.04	9.02E-03
ZSCAN1	-2.41	9.28E-03	*MYLK*	-3.10	9.14E-03
TMPRSS7	-2.42	9.93E-03	*PPARGC1A*	-4.81	9.75E-03
REG1P	-2.83	9.97E-03	*FGF1*	-5.36	9.96E-03